Application of two-dimensional materials in perovskite solar cells: recent progress, challenges, and prospective solutions

Syed Ossama Ali Ahmad, Atif Ashfaq, Muhammad Usama Akbar, Mujtaba Ikram, Karim Khan, Feng Wang, Muhammad Ikram and Asif Mahmood

Ali Ahmad, S. O., Ashfaq, A., Akbar, M. U., Ikram, M., Khan, K., Wang, F., Ikram, M., Mahmood, A., (2021), Application of two-dimensional materials in perovskite solar cells: recent progress, challenges, and prospective solutions, *Journal of Materials Chemistry C*, 9(40), 14065-14092.
https://doi.org/10.1039/d1tc02407h

ARTICLE

Application of Two-dimensional Materials in Perovskite Solar Cells: Recent Progress, Challenges and Prospective Solutions

Received 00th January 20xx,
Accepted 00th January 20xx

DOI: 10.1039/x0xx00000x

Syed Ossama Ali Ahmad,[a] Atif Ashfaq,[a] Muhammad Usama Akbar,[a] Mujtaba Ikram,[b] Karim Khan,[c] Feng Wang,[d]* Muhammad Ikram,[a]* Asif Mahmood,[e]*

Perovskite solar cells (per-SCs) with high performance and cost-effective solution processing have been the center of interest for researchers in the past decade. Power conversion efficiencies (PCEs) have been gradually improved up to 25.2% with relatively improved stability, which is an unparalleled progress in all generations of solar cell (SC) technology. However, there are still some prevailing challenges regarding stability and upscaling of these promising devices. Recently, 2D layered materials (LMs) have been extensively explored to overcome the prevailing challenges of poor stability (under moisture, light soaking and high temperature), halide segregation, hysteresis, involvement of toxic materials (i.e. lead) and upscaling of devices. A critical review addressing the recent developments in the use of 2D materials, especially transition metal dichalcogenides (TMDCs) is hence necessary. Development of novel synthesis and deposition techniques including liquid-metal synthesis and ultrasonic assisted spray pyrolysis has offered more efficient fabrication of 2D-LMs with controlled thickness and morphology. Effective functionalization approaches to increase the dispersability of 2D-LMs in non-polar solvents has boosted their potential application in solar cell technology as well. Moreover, compositing 2D TMDCs with suitable organic/inorganic compounds has enable superior charge kinetics in all functional parts of per-SCs. Additionaly, newly developed materrials suchas graphyne and graphdyine along with 2D metal organic frameworks (MOFs) and covalent organic frameworks (COFs) have been employed in per-SCs to acheve PCEs upto 20%.This review summarizes the recent progress and challenges in application of 2D-LMs in per-SCs and outlines the future pathways to further extend the PCE of per-SCs beyond 25%. This review particularly focuses on 2D-LMs as electrode materials and additives, the underlying charge (electron-hole) transport phenomenon in the functional layers and their chemical and structural stability.

1. Introduction

Perovskite solar cells (per-SCs) get their name from a well-known mineral calcium titanate ($CaTiO_3$) named as perovskite, since they have a similar structure as that of $CaTiO_3$[1]. Perovskite structures are represented by the generic formula ABX_3, where A and B are cationic species while X represents the anionic component. A cuboctahedral geometry is formed by 12-coordinated (X) A site while the B site forms an octahedral structure with 6-coordinated X species, in a perovskite structure. The unique property of accommodating large sized cations makes perovskite materials highly suitable for fabrication of organic-inorganic SCs. Conventionally, per-SCs are categorized as normal (n-i-p) and (p-i-n) devices based on direction of incident light transmission [2]. Just like dye-sensitized (DSSCs) and organic solar cells (OSCs), per-SCs can be easily converted into flexible, portable and cost effective power devices, along with high yielding solution based fabrication [3–6]. Intensive academic and industrial research work therefore, have been reported on development and advancement of per-SCs in last 10 years. Significant improvements in power conversion efficiency (PCE) of per-SCs (3.8% to 25.5%) have been made from 2010-2020, competing with silicon based SCs[7]. Excellent optoelectronic features that make per-SCs highly desirable include adequate band gap, large absorption coefficient, longer diffusion lengths, exceptional charge mobility and lower exciton recombination rate [8–12]. Regardless of these magnificent properties, there are still some limitations regarding stability, environment friendliness and PCE of per-SCs for their practical and commercial use [13,14].

Recently, researchers have diverted their attention on two-dimensional (2D) layered materials (LMs) to be used in solar cell technology for enhanced PCEs and stability, especially after the discovery of graphene (GR) as a counterpart of bulk graphite [15]. Compared to their bulk forms, these 2D-LMs exhibit outstanding optical and mechanical properties, which make them highly favourable for diverse applications. Moreover, this particular family of materials is growing rapidly, with more than 150 materials that can be transformed into 2D monolayers, already discovered and explored [16–19]. These 2D-LMs mainly include silicene (2D silicone), MXenes (2D nitrides/carbides), germanene (2D germanium), hexagonal boron nitride (h-BN), borophene (2D boron) and transition metal dichalcogenides (TMDCs) like WS_2, WSe_2 and MoS_2 [20–24].

[a] *Solar Cell Applications Research Lab, Department of Physics, Government College University, Lahore, 54000, Pakistan*
[b] *Institute of Chemical Engineering and Technology (ICET), University of the Punjab, Lahore, 54000, Pakistan*
[c] *School of Electrical Engineering & Intelligentization, Dongguan University of Technology (DGUT), Dongguan, 523808, Guangdong, China.*
[d] *Department of Physics, Chemistry, and Biology (IFM), Linköping University, Linköping SE-581 83, Sweden*
[e] *School of Chemical and Biomolecular Engineering, The University of Sydney, Darlington, Sydney, New South Wales, 2006, Australia*

Electronic Supplementary Information (ESI) available: [details of any supplementary information available should be included here]. See DOI: 10.1039/x0xx00000x

2D-LMs having large length (1-10,000 µm) to thickness (< 1 nm) ratio show highly crystalline nature. The layered structure of 2D-LMs having strong covalent bonding (intralayer) and weak van der Waals interaction (interlayer) allows brilliant electronic properties. Moreover, this layered structure permits more conductivity (3-4 times magnitude) along the layers rather than in between the layers [25–27]. Extensive research work has been conducted in exploration of such 2D materials ever since the discovery of GR and its exclusive properties [28]. High transparency, large thermal conductivities and distinct electronic band structure of GR outclassed other classes of 2D materials at that time [29]. These exceptional properties provided a significant replacement of relatively expensive Indium Tin Oxide (ITO), which is a frequently used conductive oxide in solar cell technology, LEDs and liquid crystal displays [30]. One problem however, that intrigued researchers to look for other 2D-LMs, is the zero bandgap of semimetal graphene which is not desirable in SC technology. This resulted in the discovery of new classes of 2D-LMs, especially TMDCs, which possess adequate bad gap values ranging from 1.2 to 1.8 eV that correspond well with the solar spectrum [31]. Reduction in size without compromising quality, reduced charge carriers scattering due to lesser dandling bonds and large surface to volume ratio of 2D based photovoltaic devices are highly appreciable [32,33].

Scheme 1. Overview of 2D materials; types, properties and their application in perovskite solar cells.

Various approaches have been applied worldwide, to improve the stability and PCE of per-SCs. These approaches mainly include use of low-dimensional active layers which prevents

ionic defects formation, reducing the grain boundaries by improving active layers quality, use of doped active layers and application of protective layers around active layers [34–36]. Use of carbon-based nanomaterials (C-NMs) have attracted attention of many researchers to fabricate long-term stable per-SCs, in past few years. Their inertness towards halides and water resistant nature make them highly favourable for improved stability in moist conditions [37]. Moreover, C-NMs have found variety of applications in all functional layers and interfaces of per-SCs, because of their versatile properties [38]. Furthermore, TMDCs such as MoS_2, $MoSe_2$, WS_2, and WSe_2 and $MoTe_2$ etc. with exceptional electronic and mechanical properties, have shown even better stability and PCE performance in SC technology [39,40]. Smaller diffusion lengths and reduced charge recombination rates offered by TMDCs significantly improves the efficiency of per-SCs.

In the present study, we have focused on application of 2D-LMS (especially carbon and TMDCs based materials) for improving PCE and stability of per-SCs. An overview of 2D materials is presented in **Scheme 1**. In the first section, we provide a brief overview of device structure of a typical per-SC, outline the prevailing challenges in the per-SC technology and give a brief introduction of 2D layered materials to develop a better understanding. The second section is comprised of carbon and TMDCs based based 2D nanomaterials in per-SCs and how they have been effectively utilized to address several tedious challenges. Various uses of these 2D-LMs such as HTL (hole transport layer), ETL (electron transport layer), AL (active layer), electrodes and interface modifiers have been briefly discussed.

2. Structure of per-SCs

A typical solar cell is a device made up of a semiconducting diode without any outer biasing and upon incidence of photons (light), it generates and deliver electricity to the load. The basic structure of a conventional per-SC is demonstrated in Fig. 1. Three most common parameters that are widely adopted to describe the performance of a solar cells are short circuit current (I_{SC}), open circuit voltage (V_{OC}) and fulfil or filling factor (FF). One should have a good knowledge of these key factors beforehand, in order to take maximum benefit from the contents of this feature review. The term I_{SC} corresponds to the amount of current flowing in the circuit when the voltage drop across the circuit is zero, or in other words, when the terminals of the SC are short circuited. The term V_{OC} refers to the value of externally applied voltage at which there is no net current streaming through the circuit. This is the point where the applied voltage effectively counterbalances the built-in voltage present in the device so there is no net current flowing through the circuit. The term FF is basically the ratio of maximum power (P_{max}) delivered by the SC to the product of I_{SC} and J_{SC} generated in the device. Generally, FF of a SC is given in terms of current density as,

$$\mathbf{FF} = \frac{\mathbf{J_{MP}} \times \mathbf{V_{MP}}}{\mathbf{J_{SC}} \times \mathbf{V_{OC}}}$$

Where J_{MP} and V_{MP} corresponds to the current density and voltage at which maximum power is generated by the device.

Another important factor to describe the performance of a typical SC is PCE which is the ratio of total output power generated by the device to the total optical power provided as input. It is given as,

$$\boldsymbol{\eta} = \frac{\mathbf{J_{SC}} \mathbf{V_{OC}} \mathbf{FF}}{\mathbf{P_{in}}}$$

Where P_{in} stands for the incident light irradiance and its standard value is 100 mW/cm^2 for AM 1.5 spectrum.

In the typical device architecture of a per-SC, the perovskite material is used as an active layer (AL) which is sandwiched between HTLs and ETLs layers. The overall performance which mainly include efficiency and stability of the device is highly dependent on the charge transporting materials used [41,42]. Both ETLs and HTLs play key roles in achieving a desirable performance of photovoltaic devices. The main role of these materials is to suppress the recombination of photogenic charge carriers and enhance their transportation between the AL and electrodes [43].

Figure 1: Basic Structure of a perovskite solar cell. Reproduced from Ref. [44].

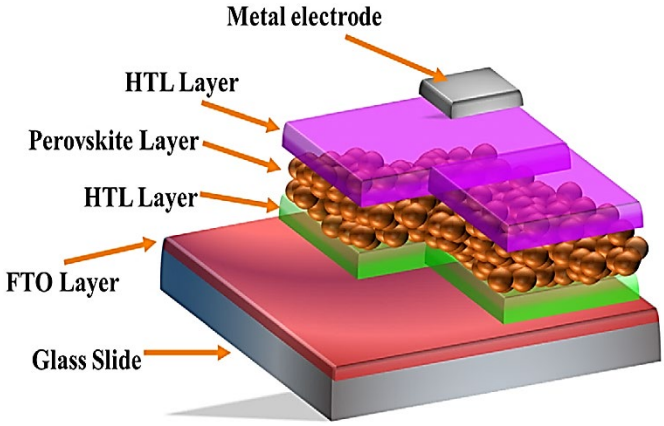

Fabrication of suitable and cost effective materials with good stability and performance to design efficient ETLs and HTLs is the paramount of solar cell technology. Researchers are vigorously looking for novel and robust materials with brilliant transport capabilities and 2D materials have recently gained intensive attention due to their exceptional properties. A great deal of research work has been reported in this regard and we believe that a comprehensive review is hence necessary to summarize the progress and development that has been achieved so far and the current prevailing challenges in the field of per-SCs. This review will help the research community and especially young researchers to have an in-depth knowledge of current challenges, in order to proceed towards more productive and fruitful ways.

3. Prevailing Challenges in per-SCs

As mentioned earlier, apart from the extraordinary development and high PCEs of up to 25.2% has been achieved by the per-SCs, this technology still faces some crucial challenges which need to be addressed. The biggest challenge however is the lower stability of perovskite materials which make them highly undesirable for long term commercial use. While evaluating the stability of perovskite devices, several degradation factors and pathways like temperature, humidity, halide concentration and dopant migration need to be addressed properly. Testing of these devices at higher temperature (above 60°C) and spontaneous heating of perovskite films under constant irradiation causes serious degradation and hence poor stability. Thermal instability of the MA cations in the perovskite film is considered to be the main reason for the thermal degradation of these devices. However, recent studies have shown that the conventionally used spiro-OMeTAD HTL plays an important role in the thermal degradation as well. At elevated temperature, spiro-OmeTAD tends to crystallize resulting in to frequent interaction of metal electrodes with the active layer of the device [45–48]. Use of carbon and TMDCs based electrodes can significantly improve the stability of the devices as they are thermally stable and can with stand higher temperature. Moreover, they do not interact with the active layers even at high temperature values [49–51].

In contrast to organic SCs, the stability of per-SCs is highly affected by the moisture which is a serious issue concerned with this technology. The degradation of per-SCs in the presence of moisture or electrolytes is ascribed to the decomposition of $MAPbI_3$ and other mixed ion active layers into lead iodide and organic iodide. Researchers have found out that these perovskite devices are even affected directly by the moisture during their assembling and testing procedures as well [52]. Formation of hydrate species have also been reported to be the reason for the degradation of perovskite active layers in the presence of moisture [53]. Several encapsulation techniques, fabrication of hydrophobic layers, use of Al_2O_3 layers and incorporation of halogens into the active layer have been reported to overcome this challenge [54–56]. But all these techniques increase the net cost of the fabricated device and use of hydrophobic 2D layered materials is an effective alternative approach in this regard. The migration of different HTL dopants like lithium through the active layer also results in the degradation of device. Moreover, the UV exposure is a crucial deciding factor to determine the stability of the per-SCs as well since it generates chemical changes in the ETL (especially TiO_2) when absorbed [57,58]. Use of materials with wider band gap and application of UV filters have depicted good results in terms of long term UV stability but they compromise the recombination rates and cost of the devices [59,60].

Apart from the above-mentioned extrinsic factors, ion migration is an intrinsic degradation factor that seriously affects the stability of per-SCs. The current-voltage hysteresis observed in per-SCs is attributed to the ion migration through the active layer [61]. Ion migration in perovskite films can lead to both slow (reversible) and fast (hysteresis) degradation of devices. The reversible losses arise due to the lattice deformation upon IR heating and can be regained after few hours of dark storage, while the latter losses results from the slower cations migration as compared to halides [62,63]. Use of carbon-based materials such as PCBM have yielded outstanding results in depleting the ion migration and various other 2D materials are being explored to be used as buffer layers as well.

One of the most important aspect in the photovoltaic (PV) technology is the correlation between materials fabrication and their performance in the designed system. Various synthetic approaches that are widely adopted for the fabrication of perovskite films and other transporting layers have significant influence on their performance. As far as the perovskite based active layers are concerned, it is very necessary to develop a deep understanding of the crystallization process of perovskite materials. It is extremely crucial in tuning the morphology and structure of these active materials to gain optimum

performance out of them. Although, the deposition techniques allow complete coverage of the substrate's surface with active material to enhance the PCE of SCs, it is yet insufficient as far as the required standards are concerned. Intensive research has revealed that the maximization of crystal domain by prolonging the crystal growth time periods via various crystallization strategies is extremely necessary to boost the performance of perovskite active layers [64]. Several crystallization techniques such as, heterogeneous crystallization, reverse temperature crystallization and solid-liquid complex formation for solution based processing of perovskite materials have been reported to achieve better control over thickness and morphology. However, there is still a lack of in-depth understanding of mechanisms lying behind these procedures and more robust studies are required for developing authenticity and integrity [65]. Recent developments in one-step solution processing of active materials in per-SCs have revealed that use of various anti-solvents such as isopropyl alcohol, benzene, chlorobenzene, chloroform, toluene and xylene result in faster nucleation to generate micro-sized crystals [66]. Furthermore, use of various lead precursors such as $PbCl_2$, PbI_2, and $PbAc_2$ seem to have significant effects on the crystallization phenomenon as well [67–69]. However, controlling the one-step processing methods is relatively difficult in contrast to deposition techniques, in case of both planar and mesostructured TiO_2 substrates among others [70]. Moreover, the fast crystallization or nucleation of active materials result in poor orientation which greatly affects the photovoltaic performance. On the other hand, solid-liquid complex formation offers high degree of orientation due to slower crystallization generated from the formation of complex bonds between solvent and precursors. However, films formed through this method does not exhibit as much performance which is a troublesome issue [71]. Although, two-step processing have helped to overcame many challenges but there are still some crucial challenges that need to be addressed. Especially, the issue of Ostwald ripening which generate relatively large crystals on perovskite films is big issue faced by two-step processing [72].

Several vapour deposition techniques are also widely adopted to produce high quality perovskite films and these techniques also generate the possibility of fabricating flexible devices [73]. However, there are a few prevailing challenges regarding the varying affinities of perovskite films with different substrates which hinders the initial formation of films and there is a need to develop intensive research on the physisorption and adsorption mechanisms of these active layers on different substrate materials in order to generate adequate crystallization. Furthermore, the challenges regarding the reproducibility of these devices are usually ignored and researchers need to focus more on the reproducibility of perovskite based devices as well. In short, the main challenge regarding the fabrication and performance of materials is the synthesis of high quality active layers with low temperature adequate crystallization to promote performance and cost durability of per-SCs.

These are some of the crucial limiting factors in the field of per-SCs technology. Researchers have been looking for various robust methods to overcome these challenges and hence 2D materials are being extensively explored in this regard. Unique optical and morphological features of these 2D-LMS along with availability of a wide range of synthetic procedures enable them as a potential candidate to improve the stability as well as the efficiency of the per-SCs. In the following sections, we have discussed in detail how 2D-LMS have been utilized in per-SCs to overcome the above-mentioned challenges. Furthermore, the emerging class of 2D-LMS i.e. TMDCs have been discussed in detail since they offer many dominating advantages over carbon based LMs as well.

4. A Brief Introduction of 2D-LMS

In the early 1900s, 2D materials and their existence had been the centre of discussion in the research community. As far as the classical physicists are concerned, they strictly believe in the thermodynamical instability of 2D materials at any temperature value which is owed to the thermal fluctuations present in their lattices [74,75]. This statement was greatly evidenced by the observation that upon reducing the thickness of 2D layered materials, the melting temperature significantly decreased. However, lateral advancement in the spectroscopic techniques helped in the discovery of 3D materials having layered structure which initially included graphite and molybdenum disulphide (MoS_2) followed by many others. However, at that time, exfoliating these bulk materials into their corresponding 2D monolayered structures seemed to be possible in the theoretical domain only [76]. The noble prize winning discovery of Novoselov and Geim to isolate monolayers of GR from its bulk structure (graphite) brought about revolutionary changes in the field of material science, in 2004 [77]. Further developments in various exfoliation methods have led to the successful isolation of almost every layered bulk material in to monolayered structures [78]. A huge variety of compounds including halides, hydroxides, chalcogenides, clays, carbides, layered oxides, hydrides, nitrides, phosphonates and phosphates are known to have layered structures. Majority of the mentioned materials possess binary layered structures however, ternary layered structures such as $CuSbS_2$ have also been manufactured [79]. Based on the nature of interaction such as, hydrogen bonding, London dispersion forces or interstitial cationic interaction among the layers, these layered materials are further categorized.

Ever since their successful exfoliation, 2D layered materials such as hexagonal boron nitride (h-BN), silicene, graphitic carbon nitride (g-C_3N_4), transition metal dichalcogenides (TMDCs), back phosphorous (BP), MXenes, GR and its derivatives have gained great enthusiasm and attention from the research community. Owing to their intriguing and novel properties (mechanical, optical and electronic) and their potential new applications, they have received considerable attention from the researchers of numerous fields including nanotechnology, chemistry, material science and condensed matter physics. For instance, the confinement of electrons in two dimensions has imparted fascinating electronic features to these 2D layered materials, boosting their potential for dynamic application in the field of electronics. Additionally, the large surface area of these compounds offer greatly improved applications regarding surface activeness such as sensing and catalysis. Moreover,

large anisotropy and extremely small thickness of 2D materials impart great optical and mechanical properties for fabrication of efficient wearable and opto-electronic systems. Furthermore, they offer easy assembling to form various heterostructures with no processing compatibility and lattice matching limitations, which benefit a great number of applications involving synergistic effects.
Although, great developments have been made in the domain of 2D layered materials, however, there are still some prevailing challenges that need to be addressed properly. High quality production at large scale with efficient control over structure is yet to be achieved for the successful commercialization. Moreover, efforts need to be made in order to correlate their structural features with corresponding properties by developing defined control over their thickness, defects, doping, compositions, surface properties, vacancies, strains, crystal phases and lateral sizes. Besides, several other non-layered 2D materials such as 2D perovskites and metal nanomaterials seem to possess fascinating properties which need to be explored as well. Several informative reviews are available on the synthesis and properties of 2D materials which provide great insights for the research community to further explore these materials. For instance, Cheng et al. have presented a detailed review on the recent developments and challenges regarding the chemical vapor deposition (CVD) based synthesis of various 2D materials. Different types of CVD grown 2D materials including single crystal, continuous and 2D heterostructures along with their potential applications were briefly reviewed [80]. Li et al. reported a comprehensive review on the growth mechanisms involved in the CVD fabrication of TMDCs and elaborated the ability to generate high quality TMDCs films with controlled thickness and brilliant electronic properties [81]. Cheon et al. have briefly discussed the solution-based synthesis of 2D layered TMDCs and highlighted several advantages such as easy solution processing, cost effectiveness, molecular level control over composition/size and scalability [82]. Feng et al. gave insights into the interface assisted fabrication processes for the production of organic and inorganic 2D layered materials and summarized numerous advantages of these synthetic approaches along with suitable characterization tools for better understanding of 2D materials [83]. Similarly, several feature reviews based on recent advances and challenges in the field of 2D layered materials including organic, inorganic, non-layered, metal 2D nanomaterials and their applications in electrocatalysis, photocatalysis and electronics among others, are available [84–87].

5. Carbon-Based 2D-LMS

Carbon-based nanomaterials (C-NMs) depict different chemical and physical properties based on various structures [88]. Generally, C-NMs are divided into four categories depending on their application in per-SCs that include carbon nanotubes, fullerenes and their derivatives, GR and its derivatives and graphite/carbon black [89]. Since this study deals with study and application of 2D-LMS only, so we will only discuss the role of GR and its derivatives in per-SCs.

5.1. Graphene and its derivatives in per-SCs:

Graphene is a sheet comprised of sp^2 hybridized carbon (C) atoms packed into 2D honeycomb crystallites. With some modifications, it can be enfolded to (0D) structured fullerenes, rolled up to obtain (1D) carbon nanotubes and stacked to form (3D) graphite [90]. Till now, different approaches such as metal-doped cathode layers, perovskite layers (surface modified), electrode modification, plasmonic NPs and unprecedented introduction of GR based composite within device layers has been carried out to improve performance and stability of per-SCs [91]. Much consideration has been given to graphene based per-SCs as it offers low cost production, greater chemical stability and impressive device designs [92]. GR with its derivatives has been used in several per-SCs with different roles due to its impressive properties, as electrode, ETL and HTL.

5.1.1. As HTL:

GR has been used in per-SCs as HTL because of impressive photovoltaic performance. GR plays an important role in per-SCs stability, particularly in device structure and because of its hydrophobic properties, thermal stability and resistance against ion migration [89]. Comparatively, because of better alignment with valance band (5.4 to 6 eV) of $MAPbI_3$ active layer (AL), graphene oxide (GO) based materials are most appropriate for per-SCs as HTL than graphene. GR can be easily processed by solution based cost effective method [46,93]. Normally work function of GO is 4.9 eV that is greater than pristine GR (4.5 eV). Greater work function will create ohmic current, increasing V_{OC} while higher conductivity will result in greater FF owing to enhanced charge collection [94].
It is a great challenge to have conductivity and higher work function for GO. This material consists of numerous functional oxygen groups which results in high work function but, more oxygen causes poor conductivity which is a limiting factor for hole transfer. Thus, for improved activity, conductivity and work function of GO must be balanced carefully [95]. Reduced graphene oxide (RGO) have been utilized as promising agent for overcoming this disadvantage [96]. Owing to excellent electrical features, GR derivatives especially RGO can be applied as a sole HTL with no need of any doping, in photovoltaic devices. Facile solution processing routes have been thus utilized to employ RGO HTLs in inverted per-SCs to achieve high stabilities and comparable efficiencies in contrast to other traditional HTLs [97,98]. However, sole utilization of RGO HTLs to achieve higher efficiencies in per-SCs has been seldom reported since full covering of perovskite layer with polar solvents processed RGO films is much difficult without damaging their structure. Few efforts have been made to successfully utilize sole RGO films in inverted per-SCs in the past. For instance, Carlo and colleagues applied an IPA-processed sole RGO film in a perovskite device via spray- and spin-coating routes. However, the fabricated device employing IPA-processed RGO HTL exhibited a poor efficiency of 6% only. The poor performance was attributed to the damaging of perovskite layer caused by the polar solvent IPA [99].
To overcome this crucial problem, there is a need to develop non-polar solvents for sole RGO processing. But the presence of

several oxygen containing groups on the edges and surface makes it very difficult to process RGO in non-polar solvents due to poor dispersibility. This result in the generation of relatively thicker HTL layers over perovskite which limits the performance of the device. Hence, the use of an additional HTL such as spiro-OMeTAD or compositing with other hole transport materials become mandatory for the realization of efficient inverted per-SCs employing RGO HTLs [100,101]. The successful processing of RGO in non-polar solvents can significantly help in avoiding the use of additional HTLs or doping/compositing methodologies. Very recently, Park et al. have reported a solution for the poor dispersibility of RGO in non-polar solvents. They reported an alkylated RGO (AF-RGO) film demonstrating great dispersibility in non-polar solvent such as chlorobenzene (CB) at high concentrations (Fig. 2a-c). The perovskite layer was completely covered by the AF-RGO HTL with no damage inflicted on the AL and a high efficiency of 17% was achieved. The sole RGO HTL exhibited minimum series resistance, great hole transport and suppressed charge recombination in the fabricated device. Moreover, the device demonstrated much greater ambient stability in contrast to reference device (employing spiro-OMeTAD HTL) with a decrease of only 11% initial efficiency, after 240 h [102].

Figure 2: (a) Synthetic route of AF-RGO. (b) Schematic illustration of the per-SC structure employing AG-RGO HTL. (c) Cross-sectional SEM image of AF-RGO-based per-SC. Reproduced from Ref. [102]. (d) Illustration of the device with P3HT as the HTL, where the hole transport is slow, resulting in charge accumulation, and device with P3HT/GR composite as HTL, where hole transports to the carbon electrode quickly. Reproduced from Ref. [103]. (e) Contact Angle of different films, (1) PEDOT:PSS, (2) MoO*x*, (3) RGO and (4) MoO*x*:RGO.

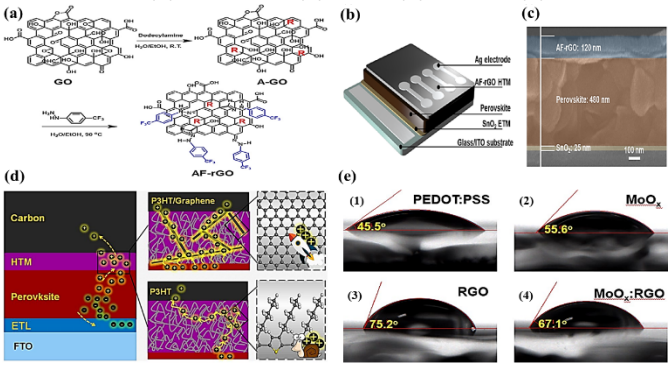

Reproduced from Ref. [104].

Chu et al. have reported a solution processed P3HT/GR nanocomposite as a modified HTL which exhibited great compatibility with paintable carbon based electrodes in per-SC. A two fold increased hole mobilities of order 1.2 x 10^{-2} cm^2 V^{-1} s^{-1} was achieved upon incorporation of GR in P3HT layers in contrast to bare P3HT. The tortuous charge transfer channels offered by the polymer film of pure P3HT result in great resistance losses and insufficient hole transfer. Addition of GR in the HTL formed well-ordered transport channels for the efficient transport of holes, as shown in Fig. 2d. The device demonstrated a high PCE of 18.1% with excellent stability by retaining 89% of its initial output after 600 h of irradiation [103]. Doping of GR was reported to improve the hole extraction abilities in traditionally used PEDOT:PSS HTL. The homogeneous layer of GR HTL obtained via spin coating resulted in a significant increase of charge mobilities without compromising the optical transmittance of the material. Furthermore, the HTL also improved the stability and crystallinity of perovskite layer grown on it [105]. Use of traditional HTLs such as PEDOT:PSS results in significant open circuit voltage losses which is a crucial challenge in the field of per-SCs. Researchers are looking for alternate organic or inorganic materials to overcome this prevailing issue. In this regard, Xie et al. reported a perovskite device employing RGO-doped molybdenum oxide (MoO_x) layers as hole transfer material. The highly conducting MoO_x:RGO HTL greatly reduced the V_{OC} losses and improved the crystallinity of active layer as well. Doping of RGO enhanced the work function of MoO_x layers and improved their hole mobilities significantly. A high V_{OC} of 1.12 V with a PCE of 18.15% was achieved which was owed to the heightened work functions of the layers upon RGO doping. Authors also stated that the contact angle of MoOx films was effectively increased upon RGO incorporation (Fig. 2e) which offer lesser nucleation sites to promote better film growth of perovskite [104].

Habib et al. studied the effects of various doping concentrations of PANI:GO nanocomposites on the hole transfer properties of the HTL in inverted per-SCs. Based on the Hall Effect evaluations, the lowest film resistance of 6.7 x 10^2 Ωcm^{-2} was shown by the 1:0.5 doping concentrations of PANI:GO composites. A further increment or decrement in GO concentration resulted in an increase of series resistance and poor hoe extraction performance [106]. Zhou et el. used a MOF-derived 2D porous carbon material enriched with nitrogen (NPC) as an additive for Li-TIFL-doped spiro-OMeTAD HTLs. Addition of NPC effectively optimized the layer quality and hole transport by reducing the number of defects and prohibiting the formation of Li salts in the HTL. Furthermore, hydrophobicity and porosity of NPC increased the stability of the device by preventing the erosion of HTL from moisture. An excellent PCE of 18.12% along with 85% retention of initial output after 720 h of air exposure was demonstrated by the prepared device [107].

Similarly, Palma et al. utilized reduced GO in mesoscopic per-SCs as a hole transport surface and experienced an enhancement in lifetime of device (1987 h). While Spiro-OMeTAD based devices exhibited decreased efficiency of about one order magnitude [108]. Similarly, Wu et al. and Li et al. utilized GO as a replacement of PEDOT:PSS (having poor stability and inefficient electron blocking potential) in HTL with enhanced crystallization of AL in p-i-n heterojunction and better surface coverage [109,110]. A further enhancement in performance of per-SCs was gained by using solution based fluorinated reduced graphene oxide as HTL. Via this process, Yeo et al. obtained PCE up to 10.0% for the fabricated device. The molecularly doped RGO promoted AL crystallization and exhibited a rapid charge extraction ability. It is quite interesting that per-SCs were fabricated at a polyethylene napphthalate (PEN)/ITO substrate which showed 8.1% PCE [111].

5.1.2. As an Electrode:

To optimize the functioning, GR has been used as electrode (cathode and anode) in several per-SCs. GR is being used as electrode in different semitransparent per-SCs. You et al. fabricated a GR layer by CVD on CU foil and then coated it by a poly (methyl methacrylate) layer and thin poly (dimethylsiloxane) was used as supporting layer [112]. For enhancing the functioning of GR as electrode, Liu et al. inserted thin PEDOT:PSS layer on the surface of GR to act as an adhesive film for perovskite film. This resulted in not only reduced film resistance, but also induced p-type dopant in GR electrode. The obtained device with double layer of graphene exhibited 11.65% as compared to pristine GR and 12.02 % from fluorine doped tin oxide [113]. However, hydrophobic GR nature causes a lot of challenges because of wettability for its application in per-SCs as an electrode [114]. Although synthesis of GR via CVD method gives superior-quality films, GO reduction is still a much cheaper synthesis technique. Yan with his team implemented single and multi-layered GR obtained from the reduction of GO as hole electrode (hole extraction) in per-SCs. In case of hole extraction, multi layered (5.0 eV work function) GR worked better than single layered (4.8 eV work function) GR because of as-formed Schottky barrier. Multi layered GR and AL interface accumulated as Schottky junction with rectifying characteristics, which supported electron rejection and hole extraction effectively, while interface of single layered GR with AL showed ohmic behavior [115].

One special property of GR as the electrode is possible chemical functionalization. For example, Shin et al. employed 3-aminopropyl triethoxysilane (APTES)-treated GR as transparent electrode to enhance the combination with ETL of graphene quantum dots (QDS) doped phenyl C61 butyric acid methyl easter for flexible per-SCs. With the increase of GR QDs concentration to 2.5mg/L, PCE increased up to 16.4 and 15% on a rigid, flexible substrate, respectively with GR/APTES TCE because of reduced recombination of charge carriers at ETL/perovskite interface and improved ETL conductivity. The per-SCs exhibited impressive bending stability maintaining at approximately 80% of original PCE after 3000 bending cycles [116]. It was found that nitrogen doping can further enhance the performance of devices. Hui et al. developed nitrogen doped GR QDs for achieving photoluminescence quantum yield to effectively convert UV light to visible photons for the sake of improving per-SC efficiency. When it is inserted on γ-$CsPbI_3$ per-SCs, it acts as energy down shift layer for harvesting light in shot wavelength (<350 nm). As a result, PCE of the prepared device improved up to 16.02% as compared to the device having no nitrogen doped GR QDs15.03% [117].

The high transparency and two-dimensional morphology make GR as an attractive candidate as a transparent electrode. Jeon et al. used GR as transparent carbon electrode and compared its performance with CNT and ITO-based bottom electrodes. PCEs reported were 14.2% and 12.8% for GR and CNT based per-SCs, respectively. Therefore, advanced methods for the preparation of GR would increase capacity of GR based per-SCs [118]. To enhance mobility, AuCl3 has been employed as a p-type dopant for transparent GR electrode (TCE) and 17.4-17.9% PCEs was achieved under one sun condition. [119]. Yoon et al. utilized GR as TCE to fabricate a flexible per-SC having structure PEDOT:PSS/GR-Mo/PEN) and determined its stability against repeated bending. Upon strain free condition, device having conductive GR electrode showed 16.8% PCE, which actually kept approximately 90% of its initial value after it was bent 1000 times (R = 2 mm) (Fig. 3). However, the reference device significantly failed with PCE reduced from 17.3 to 4.3% which was ascribed to the fracture produced in ITO layer [120].

Figure 3: (a) Normalized PCE of GR-MoO_3/PEN and ITO/PEN devices measured after 1000 bending cycles at radii of flat, 2, 4, and 6 mm, (c) Normalized PCE measured as a function of bending cycles with fixed bending radius of 4 mm. (b, d) Cross-sectional SEM images (200 nm) of MAPBI3 perovskite films coated on PEN/ ITO/PEDOT:PSS and PEN/GR-MoO_3/PEDOT:PSS, respectively after 1000 bending cycles (4 mm). Reproduced from Ref. [120]

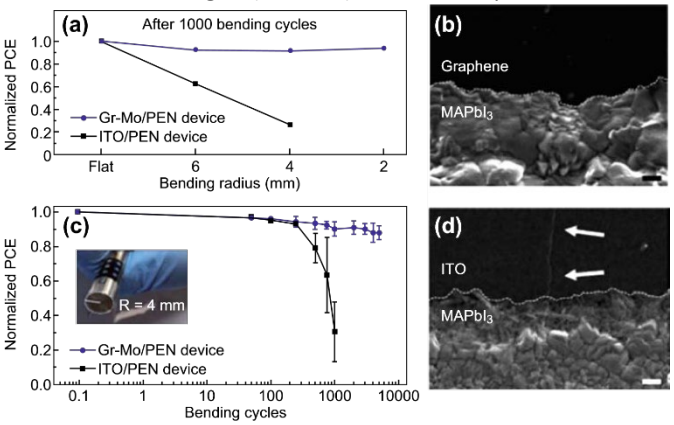

Solution based conductive transparent GR films has also been firstly tried by Munkhbayar et al. as alternative to TCO electrode at electron collecting layers on per-SCs. By optimizing and investigating tradeoff between sheet resistance and transparency of GR films, PCE of 0.62% was obtained. This further increased to 0.81% via incorporating GR into compact and mesoporous layers of TiO_2 [121].

5.1.3. As an ETL:

Stability and performance of per-SCs depend upon the type of ETL used [122]. ETL plays an important role in performance of per-SCs as it facilitates the withdrawal of photogenic excitons from ETL and transfer them to attached electrodes. Due to the resistance to chemical degradation and super hydrophobic properties, GR is attractive for improving the stability of per-SC. The GR insertion in ETL of several per-SCs has been reported to facilitate the electron transfer. Yang et al. fabricated a perovskite solar cell with GR-doped TiO_2 employed as an ETL. The optimized transport ability here is attributed to the enhanced electronic mobility produced from the addition of GR. Graphene incorporation in TiO_2 layer efficiently developed its mobility which was confirmed via Hall Effect measurements [123]. Gi-Hwan et al. fabricated a per-SC having edge selectively fluorine functionalized GR nano platelets having p-*i*-n structure

and achieved 82% stability with respect to the initial performance over almost 30 days of exposure (air) without any encapsulation. [124].

Besides, GR-based materials have been employed as additives to reduce the needed annealing temperature of present inorganic ETLs, which is critical for applications on flexible substrate of plastic and multi junction architectures [125]. Wang et al. fabricated low temperature per-SCs by developing mesostructured per-SCs with ETL consisted of anatase-TiO_2 NPs and GR nanoflakes. These GR nanoflakes provided superior charge density to the nanocomposites and enabled low temperature (150 ^oC) fabrication of the device as well. The lower temperature reduces the recombination losses and series resistance of the system. Device shows up to 15.6 % PCE with 21.9 mA/cm^2 J_{SC}, 73% FF and 1.05 V V_{OC}. Different per-SCs based only on GR, TiO_2 at high temperature and only TiO_2 exhibited 5.9%, 14.1% and 10% PCEs, respectively. This study showed that GR based per-SCs can be fabricated at low temperature to acquire high PCE [126]. Besides, the incorporated GR has the potential to facilitate charge transport and extraction. Han et al. reported RGO doped TiO_2 nano composites in processed mesostructured per-SC which showed an enhanced electron transporting property, owing to reduced resistance. This device depicted improved charge collection behaviour and fastened the diffusion coefficients which is ascribed to the higher charge mobility of RGO. Amount of RGO added to TiO_2 based ETL was optimized and their effect on electron diffusion, photovoltaic performance, resistivity and electron diffusion were improved relative to the device having just TiO_2 nanocomposites. RGO doped TiO_2 exhibited an improved PCE of 14.5% [127]. Graphene has also been tried to dope another popular ETL-SnO_2. For instance, Zhao et al. incorporated nanocrystals of SnO_2 in naphthalene diimide-GR, for highly planar per-SC as an ETL. The modified SnO_2 with high conductive 2D naphthalene diimide-GR form van der Waals forces interaction between surfactant and perovskite and increase surface hydrophobicity. This results into having 20.2% PCE with improved FF 82%. This enhanced FF and PCE was ascribed to the addition of SnO_2 doped naphthalene diimide-GR which offered better charge extraction and transport [128].

Chen et al. utilized GR/$SrTiO_3$ nanostructures as an ETL, because of superconductivity of GR along with tuning the amount of starting GR for increasing the photo harvesting ability of absorber and decreasing recombination rates. The device gained a great achievement by exhibiting PCE of 10% with 18.08 mA/cm^2 current density [129]. Kyung et al. utilized RGO in TiO_2 mesoporous layer which enhanced charge transport and its injection with layer of TiO_2 uplifted PCE to 19.54% [130].

Another approach in modifying the ETL is to introduce a monolayer of GR at the interface of the perovskite absorber and ZnO ETL. Monolayer of GR not only enhanced carrier extraction and photovoltaic properties but also saved ETL from decomposition at high temperature which improved device stability [131]. Mahdi et al. demonstrated enhanced photovoltaic stability and performance via introducing monolayer of GR at interface of perovskite absorber and ZnO ETL. This resulted in a stable electric PCE of 19.81%. Graphene QDs have also been tried as an interlayer between $MAPbI_3$ layers and mesoporous TiO_2 for fast electron extraction. The device boosted PCE from 10.15 to 98.81% with higher V_{OC} and J_{SC}. IPCE (incident photon to current conversion efficiency) spectrum represented a higher current efficiency by photons in the presence of GR QDs. According to absorption measurements, speed of electron extraction varied from 90-106 ps and 260-307 ps with and without GR QDs, respectively [132]. Agresti et al. also fabricated a per-SC having a lithium neutralized layer on TiO_2 substrate to improve electron extraction into mesoporous TiO_2 [133]. This caused an improvement in FF, J_{SC} and overall PCE, due to incorporation of hydrogen atoms in GO carboxyl groups which decreased GO work function to 4.3 eV from 4.9 eV. This delivered a suitable band alignment between GO and TiO_2 [110]. Graphene is also used as carrier transport material in several per-SCs applications. Chandrasekhar et al. revealed that PCE of ZnO-based per-SCs can be enhanced by 47.5% from 7.01% after GR is doped in ZnO ETL. Enhancing the performance up to 48.0% can be ascribed to formation of superior perovskite thin film and improved electron transport/extraction using GR dopant (low surface roughness with larger grains) [134]. It is noted that hollow structured, 3D GR scaffold can also be used as interface layer absorber layers and electron transfer in per-SCs. Several photovoltaic and characterization test results demonstrated that RGO scaffold enhanced carrier transportation and yielded 27% enhancement in overall performance of device. PCE of 17.2% for RGO based devices has been reported with FF of 72%, V_{OC} of 1.05 V and J_{SC} of 22.8 mA/cm^2. Perovskite film in contact with large surface area and light tricking property of device is the main reason for enhanced quantum efficiency which is ascribed to the GR scaffold [135]. A list of carbon and MoS2 based 2D-LMs used in various functional layers of per-SCs is formulated in **Table 1**.

5.2. Graphyne and Graphdiyne in per-SCs

With the advancements in nanomaterial technologies, some novel derivatives of GR including graphyne (GY), graphdiyne (GDY), graphone, and graphane have been developed recently. GDY is a part of GY family; first predicted by Haley et al in 1997 and due to its exciting properties, it is considered a separate derivative of GR [136]. It comprises of two linkages of acetylene in every unit cell rather than one linkage as in GY. The two linkages in GDY double the carbon chains length connecting the hexagonal rings. Consequently, GDY does not share GY's mechanical character. It is a soft material as compared to GY or GR having 120 N/m of plane stiffness. Other two are the hydrogenated derivatives of graphene [137]. These are the promising materials and possess exclusive electronic, mechanical, chemical as well as structural properties for superior performance in applications such as energy, nanocomposite and nanoelectronics [138]. Moreover, unique characteristics of these astonishing materials have been explored in per-SCs as well, which have been stated below.

Traditionally used carbon materials have established huge potential in per-SCs owing to their stability and electrical properties. GDY, as an emerging allotropic form of carbon, features homogeneously distributed pores, unique electronic character as compared to traditional carbon materials and endless design flexibility [139]. Owing

to these outstanding features, Kuang et al. used it as a dopant material for an ETL made up of PCBM for per-SCs. The obtained results indicated that the performance of the device was boosted by introducing the derivative of graphene. In the meantime, GDY showed the better coverage on layer of perovskite which exhibited better interfacial contact, low recombination of charges and fast electron mobility. As a result, PCE of 14.4% and a stable power output was achieved with a small hysteresis [140]. To increase the efficiency and stability of per-SCs, Li et al. successfully fabricated dual doping GDY in both zinc oxide (ZnO) and PCBM films. This scheme efficiently improved the films morphology and increased electrical conductivity. It also passivated the trap sites at interface which reduced charge recombination and a PCE of 20.0% was achieved in $MAPbI_3$ per-SCs [141]. To further extend the performance and suppress the hysteresis, Li et al. employed chlorine-substituted GDY-PCBM as an ETL. The experimental study revealed the strong connection between chlorine-substituted GDY and PCBM and exhibited accelerated electron transfer and condensed charge recombination which led to a repressed J-V hysteresis. These results were supported by DFT calculations that provided further evidence of derivate GDY formation. This study also offered new perspectives and implications for novel molecular design and achieved 20.34% PCE [142]. Recently, Yao et al. engineered a novel structure by incorporating GDY in an oxidized form into SnO_2 ETL. Due to its unique structural properties, GDY chemically bonded with uncoordinated Sn that reduced the oxygen vacancies in SnO_2 and ultimately improved transportation of electrons as well as reduced the non-radiative recombination. The work function of graphdiyne oxide doped SnO_2 films matched efficiently with perovskite conduction band (CB) and resulted in greater open circuit voltage. The prepared device established 21.23% PCE with a V_{OC} of 1.13 V, FF of 76.9%, and J_{SC} of 24.5 $mAcm^{-2}$. Moreover, encapsulated device upheld initial efficiency around 84% for 24 days at 80 ℃, and 71% of PCE for 160 h after constant illumination [143].

Optimizing the interface properties of per-SCs by engineering with 2D material offers a direction for developing competent and stable per-SCs. In this regard, graphdiyne presents huge potential for practical applications. GDY, when utilized as surface modifier can effectively stimulate the optical and electronic properties of the per-SCs. To discover such features for higher light-to-electricity conversion efficiency, multiple investigations have been done to modify the interfacial interactions and electronic properties of the devices. In this regard, Xiao et al. introduced this novel derivative of graphene as a dopant to P_3HT HTL, for the first time. A strong π–π stacking interaction occurred between GDY particles and P_3HT, favourable for the transportation of holes. Furthermore, the scattering nature of some GDY aggregates helped to improve the light absorption range of the active layer and 14.6% light-to-electricity conversion efficiency was attained, superior to pure P_3HT-based devices [144] The doping of GDY in $MAPbI_3$ per-SCs was also reported by Li and colleagues as a hole-transport material. This work improved the surface wettability and morphology with uniform coverage and suppressed grain boundaries. Instantaneously, it amplified the hole-extraction and minimized charge recombination as well as enhanced performance of device. Therefore, a PCE of 19.5% was achieved based on increased short-circuit current and FF [145]. To understand above mentioned features, a computational study has been reported by Guo et al. where they examined atomic scale mechanisms and underlying properties of GDY/$MAPbI_3$ interfaces. The heterostructure was designed on the basis of van der Waals interaction and intrinsic electronic character of GDY and perovskite were found well preserved within interface. These results supported the experimental studies and offered new insights towards the development of novel approaches for increasing the performance of per-SCs [146]. Later, Zhang et al. used GDY as a hole transport modifier in layer of perovskite for planar per-SCs. It was implanted on to the upper part of the layer of perovskite utilizing GDY-containing chlorobenzene as an anti-solvent. Surprisingly, GDY served as the hole collector and transport tunnel, thereby promoting the separation as well as diffusion of electrons and holes inside the perovskite. Consequently, compared with individual planar per-SCs, the prepared device exhibited improved Jsc and PCE and the charge recombination and dark current were efficiently retarded [147].

Apart from being used as an interface modifier or a dopant material for ETLs and HTLs, GDY has also been incorporated in the perovskite layers to enhance the light harvesting and stability of these devices. For instance, Li et al. incorporated GDY into $FA_{0.85}MA_{0.15}Pb(I_{0.85}Br_{0.15})_3$ perovskite films to form planar per-SC. Due to a significant support of GDY, photogenerated charge extraction and mobility greatly increased which improved the J_{SC} and FF. The most important finding was the anti-moisture stability of the device which could retain 95% of initial performance after 140 days, under ambient condition [148]. To cope with the issues of hysteresis and non-radiative recombination, Chen et al. introduced triazine-GDY (N rich material) into the active layer of per-SC. The presence of triazine-GDY modified grain boundaries and promoted charge extraction and transportation. It also reduced the non-radiative recombination in active layer which thus suffered very low amount of hysteresis and yielded 20.33% PCE. Moreover, when triazine-GDY was used in $FAPbI_3$ system, it yielded PCE of 21.16% [149]. After that, Bi et al. studied a model of van der Waals heterojunction formed by GDY and $MAPbI_3$ perovskite films to increase the photocurrent response near infrared region (NIR). To develop better insight, first principles calculations were used to check the electronic properties of GDY/perovskite heterojunctions. The results revealed that the transfer of charge between perovskite and GDY lead towards a built-in electric field which facilitated photogenerated charge separation and transport [150]. Recently, Huang et al. utilized fluorinated and nitrogen-doped GDY (F:N/GDY) in active layer of per-SC. The incorporation of heteroatoms turned out to be an efficient way for high performance per-SC, which increased 32.8% to 33%, better than GDY doped per-SCs. The doped GDY improved the surface and bulk crystallinity as well as reduced surface defects. The amplified efficiency was caused by F-GDY was ascribed to improvement of FF, while the J_{SC} played more significant role by N-GDY doping [151].

6. TMDCs in per-SCs

Owing to ambipolar nature, TMDCs have been utilized in various functional parts of per-SCs, especially in ETL and HTL. We can control the p and n type nature of fabricated 2D materials and TMDCs by adopting suitable growth procedures. However, the ambipolar nature usually diminishes due to chalcogen vacancies, gas absorption and oxidation. Several methods

including surface charge transfer, are adopted to induce ambipolar charge transfer in these materials. The methodology and mechanisms involved in ambipolar charge transfer in these 2D materials is beyond the scope of this article. In this section, we have discussed various applications of TMDCs in per-SCs technology briefly. Due to exceptional mechanical, electronic and optical properties, they found many applications (especially opto-electronic) in photovoltaic devices [152]. Moreover, they provide better advantages of improved thermal and moisture stability owing to unique structural and electronic properties in contrast to carbon based LMS.

6.1. MoS_2 in Per-SCs

Among TMDCs, MoS_2 has been explored most expensively for various applications. Photo-absorption for MoS_2 is in visible and infra-red (IR) region, having absorption coefficient 10^5-10^6 cm^{-1} with tunable bandgap. Moreover, reduction in thickness of MoS_2 from bulk to few layers causes a shift of indirect band gap (bulk) to direct band gap (exfoliated). Light-matter interaction in MoS_2 is robust and manifest intense photoluminescence caused by quantum confinement effect. All these mentioned features enable its utilization in photovoltaics as a buffer layer (BL), hole transport layer (HTL), as an interfacial layer, and also as an electron transport layer (ETL) [153].

6.1.1 MoS_2 in ETL

Till now, many ETLs have been fabricated, comprising metal oxides and its composites to establish better PCEs for per-SCs [154–159]. Researchers mainly focused on transition metal oxides such as zinc sulfate ($ZnSO_4$), titanium dioxide (TiO_2), tungsten trioxide (WO_3), zinc oxide (ZnO) and tin dioxide (SnO_2). TiO_2 has been proved as an efficient ETL in planar per-SCs and outperformed PCEs over 15% [160,161]. As the rate of transfer of electron from active layer to TiO_2 is rapid but it has certain limitations such as poor stability as well as high density of trap sites which results in recombination of charges at the interface of TiO_2/perovskite [162]. Another downside of TiO_2 ETL is high temperature sintering ~400-500 ^oC required to synthesize anatase phase which is electrically conducting, thus restricting its usage in flexible electronics [163]. According to several reports, SnO_2 prepared at low temperature ~180-200 ^oC [164] and ZnO prepared by spin coating at low temperature annealing ~120-150 ^oC [165,166] have been used as ETL in per-SCs and PCEs achieved is 12-15%. Severe decomposition occur on films of perovskite loaded on ZnO due to acetate ligand on the surface of metal oxide or hydroxyl groups [167]. As, SnO_2 exhibits better stability regarding environment but the major concerns about its utilization as ETL are, (i) it degrades at high temperatures and (ii) voltage loss due to its lower conduction band as compared to perovskite [168]. Some other organic composites have been employed as ETL (at temperature ≤100 °C) such as PCBM:C_{60}:PCF [169] and PEI:PCBM [170] and revealed the PCEs between 17-19%. Nevertheless, solubility of lower ETL layers causes an issue in the fabrication of per-SCs processes. Hence, in the ongoing drive to explore more efficient and stable ETLs for per-SCs, TMDCs thin layers, especially MoS_2 have attained much interest. MoS_2 thin film has multiple benefits as a transport layer due to its high flexibility and enables quick charge transportation in vertical direction. Additionally, it has fewer traps due to absence of dangling bonds on the surface of layer as well as inert (chemically) with high mobility of electron. By adjusting chemical composition, number of layers, elemental doping, and surface states, MoS_2 work function can be varied depending upon fabrication approach [171,172]. Therefore, it can prove to be a potential candidate for ETL, if its work function is comparably low than TiO_2 and SnO_2.

Currently, preparation of transport layer by MoS_2 has been attained by printing MoS_2 inks or transferring a chemical vapour deposition (CVD) grown MoS_2 film on per-SCs electrode [171–175]. Such deposited layers are thick enough in size and the vertical transport of charges is very slow. The charge transportation on to per-SCs electrode is not swift and not practical for large scale applications. Above mentioned approaches face the problem of weak adhesion with the electrode of per-SC. To resolve these fabrications issues of MoS_2 thin film, synthesis should be engineered at low temperature over a vast area without thermal annealing at high temperature. Additionally, the fabrication should be brought about directly on the electrode of per-SCs to get rid of transfer process. In 2019, Singh et al. reported the use of MoS_2 thin film as ETL in per-SCs, for the first time (to our best knowledge), in which uniform MoS_2 thin film was deposited directly on glass/FTO substrate at low temperature by microwave-assisted fabrication in solution phase as shown in Fig. 4a. This type of ETL set up thermally stable interface without any annealing treatment with the perovskite. The MoS_2 film appeared as highly transparent and conducted electrically in vertical direction having a current density ~21.7 $mAcm^{-2}$ and PCE of 13.14%. The performance was efficient enough as compared to per-SCs synthesized by SnO_2 and TiO_2 as ETL. According to their results, thin film of MoS_2 exhibits finer conductivity and healthy charge transportation at the interface of perovskite/MoS_2 layers [176]. A comparison of various parameters between MoS_2 (ETL) based per-SCs and other commonly used ETLs, is given in Table. 2;

Above mentioned thin layers of MoS_2 are inapplicable for vast scale production of per-SC due to their complicated preparation technique and bit slower charge transfer in vertical direction. Also, acquired PCE of 13% was not so excellent but comparable to other ETLs performances reported in recent years. So to avoid intricate challenges regarding formation of efficient films, there was a need to develop nanosheets of 2D MoS_2 at low temperature to assist charge transportation efficiently in vertical direction. These 2-D nanosheets having unique structures facilitate rapid transportation of charges and majorly carry few single nanosheets [177].

Mahmood et al. in 2020 tried to overcome these difficulties by employing nanosheets of MoS_2 thin films as ETL in per-SCs. Nanosheets were generated by hydrothermal process at low temperature followed by deposition of nanosheets layers through electrospray process directly onto FTO substrate. For comparison purpose, nanosheets grown by hydrothermal process were also generated over FTO by spin-coating method. As compared to spin coating method, electro-spraying technique formed the nanosheets layer-by-layer with better surface coverage. The PCE of nanosheets deposited by electrospray was 16% which was higher than spin coated nanosheets (13.93%), due to uniform coverage of surface by MoS_2 nanosheets and larger contact with perovskite layer for quick vertical charge extraction [178]. The following device fabricated with the structure of: glass/FTO/MoS_2 nanosheets (ETL)/perovskite absorber layer/HTL/Au, revealed PCE of 16.09% (average) which is higher than previously reported by Singh et al. Various factors were involved in the improvement of device performance such as better morphology, quick charge extraction at the interface of MoS_2/perovskite layer and good electrical conductance.

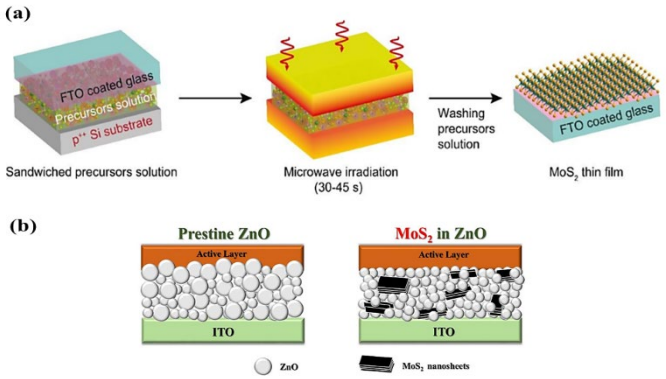

Figure 4: (a) Schematic of the microwave assisted synthesis strategy for MoS_2 thin film directly on glass/FTO substrate. Reproduced from Ref. [176]. (b) Schematic illustration of pristine and doped ZnO composite. Reproduced from Ref. [179].

Another work was reported in 2020 by Malek et al. for the fabrication of ETL by ultra-thin MoS_2 nanosheet. They adopted low cost ultrasonic spray pyrolysis method to fabricate MoS_2 ETL as compared to conventionally used methods such as liquid phase deposition, CVD, and solvo-thermal method. By this method, nanosheets were prepared with precise control through simple modification on at temperature <250 °C. MoS_2 was deposited on ITO substrate as ETL for triple cation $Cs_{0.05}[MA_{0.13}\text{-}FA_{0.87}]_{0.95}Pb(I_{0.87}Br_{0.13})_3$ perovskite absorber. The efficiency generated by this device was 3.36% with fill factor (FF) (0.370), current density (J_{SC}) (16.24 $mAcm^{-2}$), and voltage open circuit (V_{OC}) (0.56 V). These results are not as much impressive as previously reported, due to the unfortunate generation of by product impurities [180]. The performance can be enhanced by preparing high quality nanosheets of MoS_2. Apart from its application as ETL in pristine form, MoS_2 composites has also been utilized in SC technology. However, only limited work has been reported on MoS_2 composites to be used an ETL in per-SCs. Huang et al. adopted sol-gel synthesis to fabricate MoS_2 doped ZnO composites which was applied as ETL on inverted perovskite material, in 2018 (Fig. 4b). They effectively varied the band gap value of prepared composite (4.45-4.42 eV) after varying doping concentration of MoS_2 up to 0.5 wt% in ZnO. They achieved a relative increase of 15% in PCE of fabricated PTB7-TH:PCBM device with the help of MOS_2 doped ZnO(0.5 wt%) ETL [179].

Another composite of MoS_2 with TiO_2 was employed by Ahmed et al. as an ETL and absorption layer in perovskite $CH_3NH_3PbI_3$ SC. They achieved improved efficiency of 4.43% from 3.4% for the fabricated device, owing to the reduced series resistance (consequently higher current density) because of higher mobilities in MoS_2 doped ETL [181]. In another study, a thin MoS_2 layer (2-5 nm) was deposited on $PC_{61}BM$ ETL via thermal evaporation by Wang et al. to fabricate Glass/ITO/PEDOT:PSS/GO:PEGMAPbI$_3$/PCBM:MoS_2/Ag inverted device. They explained that enhancement in energy matching for HTL and Ag electrode can be improved by deposition of MoS_2 layer on ETL for efficient performance. An overall efficiency of 19.14% and large V_{OC} of 1.135 V was attained with the fabricated per-SCs [182].

6.1.2. MoS_2 in HTL

MoS_2 has been used as HTL due to excellent extraction (of holes) property, in per-SCs. Although, MoS_2 and other TMDCs are highly favourable for photovoltaic applications, owing to their outstanding properties, there are still some challenges in the fabrication of such materials. The frequently used CVD method generates highly crystalline and uniform monolayers with larger surface area, however this technique is extremely costly. On the other hand, other techniques like spray coating, drop casting and spin coating have proven to be very cost effective but they compromise the quality of the films by inducing aggregation and restacking defects. Researchers are looking for various cost-effective non-traditional fabrication routes to overcome such limitations. In this regard, Dasgupta et al. in 2017 reported a MoS_2 HTL by adopting centrifugal casting method to form single and few-layered uniform thin films of MoS_2 on large area. The fabricated sheets showed good crystallinity and fewer defects, at a relatively lower cost. Established thin film reported in this work efficiently transferred holes form $MAPbI_3$ to MoS_2 which also acted as an electron-blocking layer. The obtained PCE was ~6% (with five layers of MoS_2 nanosheet) that is significantly lower than conventional inverted per-SCs [183]. Characteristic parameters of prepared device are given in the Table. 4.

Similar challenges regarding cost effectiveness and fabrication of uniform films with larger surface area, were studied by another group. Kohnehpoushi et al. in 2018, studied MoS_2 as a potential HTL for the fabrication of more efficient and cost-effective per-SCs (Fig. 5 a,b). The key factor studied for high PCE was the thickness of MoS_2. The light absorption and photo-generated charge carriers were analysed by perovskite layer bandgap and its thickness. The optimum thickness limit for per-SCs was reported as 500 nm and further increment caused more recombination due to defects and grain boundaries of MoS_2/perovskite layer. Moreover, suitable metal back contacts were found to collect the charge carriers from TiO_2 layer such as Cu, Ag and Al with work function -4.8, 4.2-4.7, 4.06-4.24 eV, respectively. The open circuit voltage of 930 mV was obtained due to their work function which was close to conduction band of TiO_2 layer. The PCE secured by this device was ~20.43% utilizing single sheet of MoS_2. The thickness of perovskite layer and suitable metal back contacts lent unique photovoltaic properties to designed per-SCs [184].

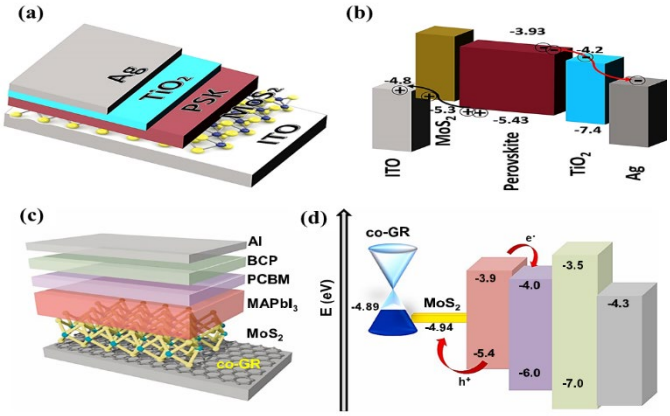

Figure 5: (a) Schematic of device architecture **(b)** and energy level diagrams for TCO/MoS_2/$MAPbI_3$/TiO_2/Ag. Reproduced from Ref. [184]. (c) Schematic device structure, (d) Energy band diagram for Glass/GR/MoS_2/$MAPBI_3$/PCBM/BCP/Al SCs. Reproduced from Ref. [185].

Another challenge that the per-SC technology face is the stability of the devices. Researchers are desperately looking for transport layers which are much stable in contrast to other traditional layers. TMDCs, being inorganic in nature can prove to be highly effective in this regard. In 2020, efforts of Shin et al. resulted in the fabrication of self-powered inverted (p-*i*-n) bifunctional per-SC with MoS_2 employed as HTL. By using CVD method, 4~5 layers of MoS_2 were deposited on polyethylene terephthalate and glass substrates. Increase in current (~10^6 times) was observed at 0 V, under light irradiation. The fabricated device exhibited PCE of 13.09% with only 38% degradation in first 30 days of working. Graphene was doped with Au on electrode for better charge extraction and performance of the device was analysed on the basis of its degradation with time (as it degraded ~38% after 30 days) along with ~57% of original photo-current maintained after 3000 bending cycles [185]. The schematic structure and energy level diagram is presented in Fig. 5c and 5d.

Despite of many overwhelming advantages, MoS_2 still suffers with the issue of extremely low solubility in many solvents. This limits the solution processed fabrication (which is very cost effective and desirable for large scale production) of MoS_2 layers. To overcome this issue, various physical and chemical blends of MoS_2 are being utilized. Dai et al. reported a blend of MoS_2 in PEDOT:PSS (a conductive polymer) used as HTL, to enhance the performance of per-SC with a PCE of 16.47%, in 2017. They proposed a metalorganic compound Phenyl Acetylene Silver (PAS) to increase solubility of MoS_2 in commonly used solvents, for cost effective fabrication. The coordination between S atoms of MoS2 and the Ag atoms coming from PAS resulted in superior solubility of the prepared blend in many solvents [186]. The traditional used material as HTL in per-SCs is made up of PEDOT-PSS, which suffers with some disadvantages. The shallow work function of PEDOT:PSS (4.9-5.1 eV) results in an imperfect Ohmic contact with the AL of the device. This significantly reduces the V_{OC} of the device due to increased recombination rate of the charge carriers at the HTL/AL interface. Furthermore, the acidic nature of PEDOT:PSS is also a big concern, since it poses the threat of corrosion to ITO layer as well. To overcome such issues, a study was reported by Wang et al. in 2018, where they incorporated a hybrid HTL of MoS_2 doped PEDOT:PSS in the inverted (p-*i*-n) per-SC. A high stability PCE of 18.5% compared to control device was reported for Glass/ITO-PEDOT:PSS/$MAPbI_3$/PCBM/BCP/Ag inverted per-SC. Doping of MoS_2 significantly increased the transport of charge carrier in HTL due to high carrier mobility of MoS_2 as depicted in Fig. 6. Moreover, 10% decrease in contact resistance was observed for MoS_2 blended PEDOT:PSS HTL, while recombination resistance was improved up to 50%, effectively [187].

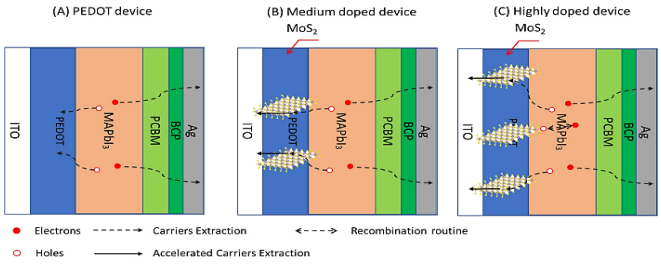

Figure 6: Schematic diagram of the charge transportation of different concentration of MoS_2 nanoflakes blended in PEDOT:PSS HTL based devices. The 2D MoS_2 introduces faster carrier extraction routes, but high concentration nanoflakes in HTL could also introduce new recombination sites. Reproduced from Ref. [187].

Table 1: Carbon and MoS_2 based 2D-LMs in various functional parts of per-SCs

Material/ Function	Method [Ref.]	Device structure	Effect	J_{SC} (mAcm^{-2})	PCE $_{max}$ (%)
Graphene/Anode	CVD [112]	FTO/c-TiO_2/$MAPbI_{3-x}Cl_x$/spiro-OMeTAD/PEDOT:PSS/GR(PDMS/PMMA/GR film)	Illumination	17.7	12.0
	CVD [114]	GR/MoO_3/PEDOT:PSS/$MAPbI_3$/C_{60}/ BCP/LiF/Al	PCE↓	21.9	17.1
	Hummer's method [121]	GR/c-TiO_2/mp-TiO_2/$MAPbI_{3-x}Cl_x$/spiro-OMeTAD/Au	PCE↓	2.55	0.62
	CVD [120]	PEN/GR/MoO_3/PEDOT:PSS/$MAPbI_3$/C_{60}/BCP/LiF/Al	PCE↓ Mechanical stability↑	21.7	16.8
	Spin-coating [188]	FTO/c-TiO_2/GR flakes+mp-TiO_2/GO-Li/$MAPbI_3$/spiro-OMeTAD/Au (large-area)	Stability↑	-	12.6
GR/Interfacial layer	Spin-coating [124]	ITO/PEDOT:PSS/$MAPbI_3$/PCBM/GNPs /Al	Stability↑	18.5	14.3
GR/ETL	Spin-coating [129]	FTO/c-TiO_2/mp-GR/$SrTiO_3$/$MAPbI_3$/spiro-MeOTAD/Ag	PCE↑	18.08	10
	Spin-coating [128]	ITO/SnO_2:NDI - GR/$FA_{0.75}MA_{0.15}Cs_{0.1}PbI_{2.65}Br_{0.35}$/spiro-OMeTAD/Au	PCE↑ Stability↑	22.7	20.2
	Spin-coating [189]	FTO/GQD@SnO_2/$Cs_{0.05}((FAPbI_3)_{0.83}(MAPbBr_{3)0.17)0.95}$/spiro-OMeTAD/Au	PCE↑	23.5	19.2
	Spin-coating [131]	FTO/ZnO/GR/LHP/spiro-OMeTAD/Au	PCE↑ Light and thermal stability↑	22.7	19.8
	Spin-coating [190]	FTO/c-TiO_2:GNRs/mp-TiO_2:GNRs/$MAPbI_3$/spiro-OMeTAD/Ag	PCE↑ Stability↑	23	17.7
GR/Electrode and ETL	Spin-coating [116]	GR/PCBM:GQDs/$MAPbI_3$/PTAA/Au	PCE↑ Mechanical stability↑	20.8	16.4
GR/EDS layer	Spin-coating [116]	N-GQD EDS /FTO/TiO_2/γ-$CsPbI_3$/ PTAA/Au	PCE↑ UV stability↑	19.2	16.2
RGO/ Interfacial Layer	Drop-casting [191]	FTO/c-TiO_2/mp-TiO_2/$FAMACsPbI_{3-x}Br_x$ /CuSCN/RGO/Au	Light and thermal stability↑	23.2	20.4
RGO/ETL	Spin-coating [131]	FTO/c-TiO_2/mp-TiO_2/$FAMACsPbI_{3-x}Br_x$/CuSCN/RGO/Au	PCE↑	22	14.5
	Electrophoretic Deposition (EPD) [192]	FTO/ZnO-RGO/$MAPbI_3$/spiro-OMeTAD/Au	PCE↑ Stability↑	21.7	15.2
	Spray-pyrolysis [130]	FTO/c-TiO_2/mp-TiO_2:RGO(Li treated)/$(FAPbI_3)0.85(MAPbBr3)0.15$/spiro-OMeTAD/Au	PCE↑	22	19.5
	Spin-coating [193]	FTO/RGO-TiO_2/RGO-$MAPbI_3$/RGO-SpiroMeOTAD/Ag	PCE↑ Stability↑	22.9	16.5
	Spin-coating [194]	FTO/c-TiO_2:RGO/mp-TiO_2:RGO/$MAPbI_3$/spiroMeOTAD/Au	PCE↑	16.5	9.3
RGO/ Interfacial Layer	Electrospray method [195]	ITO/c-TiO_2/$MAPbI_3Cl_{3-x}$/RGO/spiro-OMeTAD/Au	PCE↑	21.5	18.8
RGO/HTL	Spin-coating [196]	FTO/TiO2/$MAPbI_3$/spiro-OMeTAD+RGO/Au	PCE↓ Stability↑	16.7	10.6
	Spin-coating [197]	ITO/RGO/$MAPbI_3$/PCBM/Ag	-	21.0	16.8
RGO/HTL and Anode	CVD [115]	FTO/c-TiO_2/mp-TiO2/$MAPbI_3$/RGO	PCE↑	16.7	11.5
GO/HTL	Spin-coating [94]	ITO/PEDOT:PSS:AgOTf-dopedGO/$MAPbI_3$- xClx/PCBM/Au	PCE↑	19.2	11.9
	Spin-coating [198]	ITO/ammonia-treated GO/$MAPbI_3$-xClx/PC61BM/BCP/Ag	-	18.4	14.14
	Spin-coating [109]	ITO/GO/$MAPbI_3$-xClx/PCBM/ZnO/Al	PCE↑	17.5	12.4

GO/ETL	Spin-coating [199]	FTO/spiro-bifluorene/GO-$MAPbI_3$/$PC_{61}BM$/Au	PCE↑	18.8	14.3
	Spin-coating [200]	ITO/GO/$MAPbI_3$:GO/PCBM/Ag	PCE↑ Stability ↑	20.7	15.2
GO/Interfacial layer	Spin-coating [133]	FTO/c-TiO_2/mp-TiO_2/GO-Li/ $MAPbI_3$/spiro-OMeTAD/Au	PCE↑ Stability ↑ Hysteresis↓	19.6	11.8
	Spin-coating [201]	ITO/PEDOT:PSS-GO:NH3/$MAPbI_3$- xClx/$PC_{61}BM$/Bphen/Ag	PCE↑	21.7	16.1
	Spin-coating [202]	FTO/c-TiO_2/mp-TiO_2/$MAPbI_3$-xClx/GO/P_3HT/Au	PCE↑	24.4	13.2
MoS_2/ETL	Microwave-assisted process [176]	glass/FTO/MoS_2/perovskite/po-spiro-OMeTAD/Au	PCE ↑, Thermally stable interface↑	21.7	13.14
	Electrospray [178]	glass/FTO/MoS_2 nanosheets (ETL)/perovskite absorber layer/HTL/Au	PCE↑ Uniform surface coverage	21.0	16.17
	Ultrasonic spray pyrolysis [180]	ITO/MoS_2/ Perovskite/Spiro-OMeTAD/Au	PCE↓	16.24	3.36
	Spin-coating [179]	glass/ITO/ZnO:MoS_2/PTB7-TH:$PC_{71}BM$/MoO_3/Ag	PCE↓ Varied the bandgap	18.4	15
	Spin-coating [181]	Glass/ITO/MoS_2-TiO_2/$CH_3NH_3PbI_3$/HTL/Au	PCE↑	13.36	4.3
	Spin-coating [182]	Glass/ITO/PEDOT:PSS/GO:PEG-$CH_3NH_3PbI_3$/PCBM:MoS_2/Ag	PCE↑	22.8	19.14
MoS_2/HTL	Centrifugal casting [183]	Glass/ITO/ MoS_2/$CH_3NH_3PbI_3$/ $PC_{60}BM$/Al	PCE↓	12.3	6.0
	SCAPS simulation [184]	transparent conductive oxide (TCO)/MoS_2/$CH_3NH_3PbI_3$/TiO_2/Ag	PCE↑ Single sheet of MoS_2	26.24	20.43
	CVD [185]	Co-GR/MoS_2/$MAPbI_3$/PCBM/BCP/Al	PCE↑ Self-powered	19.97	13.09
	Spin-coating [186]	Glass/ITO/PEDOT:PSS-MoS_2/$MAPbI_3$/PCBM/Ag	PCE↑	24.03	16.47
	Spin-coating [187]	Glass/ITO-PEDOT:PSS/$MAPbI_3$/$PC_{71}BM$/BCP/Ag	PCE↑	21.33	18.5
MoS_2/BL	Spin-coating [203]	glass/FTO/ compact-TiO_2/mesoporous-TiO_2/$CH_3NH_3PbI_3$/MoS_2/SpiroOMeTAD/Au	PCE↑ Stability↑	18.8	13.3
	Spin-coating [204]	Glass/ITO/PEDOT:PSS/MoS_2/$CH_3NH_3PbI_3$:MoS_2/PCBM/Bphen/Ag	PCE↑	21.19	18.31
	Spin-coating [205]	Glass/ FTO/compact-TiO_2/ mesoporous-TiO_2/$FA_{85}MA_{15}PbI_{85}Br_{15}$/2D MCs/Spiro-OMeTAD/Au	PCE↑ Stability↑	21.64	14.9

Table 2: Relevant photovoltaic properties of the solar cells with different ETLs. Averages were taken over eight devices [176].

ETL	**V_{OC}(V)**	**J_{SC} (mA cm^{-2})**	**FF (%)**	**PCE (%)**	***PCE_{max}***
FTO	0.71± 0.005	17.4 ± 0.18	46.2 ± 1.52	5.78 ± 0.33	6.11%
MoS_2	0.89± 0.003	21.7± 0.35	46.2 ± 1.52	12.68± 0.46	13.14%
SnO_2	1.04± 0.003	22.4± 0.31	66.7 ± 0.78	15.58± 0.22	15.80%
TiO_2	1.06± 0.005	22.9± 0.19	69.6 ± 0.96	16.89 ± 0.26	17.15 %

Table 3: Device parameters obtained in different scanning modes for MoS_2 nanosheet ETLs deposited both by electrospray and spin-coating methods, under one Sun illumination (AM 1.5G, 100 $mWcm^{-2}$). Reproduced from Ref. [178]

Process	Scan direction	V_{OC} (mV)	J_{SC} ($mAcm^{-2}$)	FF (%)	PCE_{avg} (%)	PCE_{max} (%)
Electrospray	Reverse	980	21.0	69	14.30 ± 0.11	16.17
	Forward	980	20.8	69	14.06 ± 0.12	16.02
	Average	980	20.9	69	14.13 ± 0.11	16.09
Spin-coating	Reverse	965	19.0	66	12.10 ± 0.12	13.93
	Forward	965	18.5	66	11.78 ± 0.12	13.65
	Average	965	18.75	66	11.94 ± 0.12	13.79

Table 4: Photovoltaic parameters of $MoS_2|MAPbI_3|PCBM$ heterojunctions having different number of MoS_2 layers. Numbers in the parentheses denote the average value of respective parameters and their standard deviation. Since there was little variation in V_{OC} its standard deviation has not been shown. Reproduced from Ref [183].

No. of MoS_2 layer	V_{OC} (V)	J_{SC} ($mAcm^{-2}$)	FF (%)	PCE_{avg} (%)	PCE_{max} (%)
0	0.62	(8.3 ± 0.7)	(30 ± 1.2)	(1.53 ± 0.2)	1.76
3	0.83	(9.1 ± 0.7)	(42.9 ± 0.5)	(3.20 ± 0.3)	3.52
4	0.83	(10.8 ± 0.4)	(48.3 ± 0.4)	(4.2 ± 0.3)	4.54
5	0.84	(12.3 ± 0.3)	(56.6 ± 0.4)	(5.8 ± 0.2)	6.01
6	0.84	(9.5 ± 0.6)	(51.2 ± 0.3)	(4.1 ± 0.2)	4.34

6.1.3. MoS_2 in buffer layer

Apart from its advantageous use as ETL and HTL in per-SCs, MoS_2 has also been utilized as buffer layer (BL) to prevent degradation and improving stability of device. Although, work reported on the use of MoS_2 as BL in per-SCs is limited but is very yielding and offer more opportunities in this regard for researchers to explore. Due to the lower stability of Spiro-OMeTAD HTL, researchers have been exploring for other materials as a replacement. But no suitable replacement that can match the ideal positioning of Spiro-OMeTAD band edges, has yet been found. Another proposed solution to this challenge is the use of protective or buffer layers between the HTL/AL for improved stability of device. TMDCs can prove to be ideal candidate for such kind of applications in photovoltaics. To our knowledge, the first use of MoS_2 as BL in per-SCs for long term stability of device, was reported by Capasso et al. in 2016. They utilized MoS_2 nanoflakes in the interface to prevent Iodine migration from AL to HTL and direct interaction of electrode contacts with AL (which prevents recombination losses) in per-SCs. They achieved a device with PCE of 13.3% having long term stability of more than 550 hours [203]. Liu et al. has recently

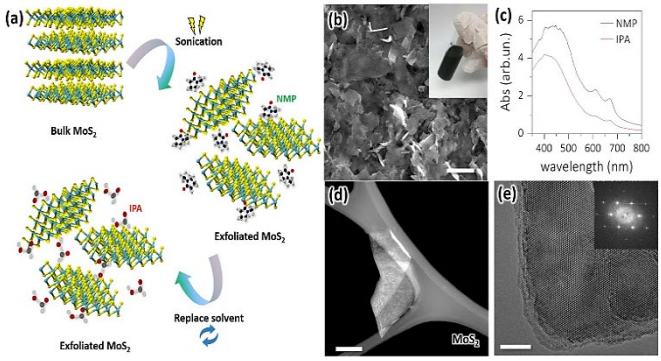

fabricated a stable device with MoS_2 BL, showing an efficiency of 18.31%. Due to suitable configuration of energy levels, MoS_2 sheet acted as a BL at perovskite and HTL interface, effectively reducing recombination of excitons by hindering the transmission of electrons. Consequently, they overcame the issue of acidity and hydrophobicity of PEDOT:PSS (poly 3,4-ethylene dioxythiophene:poly styrene sulfonate) HTL based per-SCs by fabricating a more stable and efficient device with Glass/ITO/PEDOT:PSS/MoS_2/$CH_3NH_3PbI_3$:MoS_2/PCBM/Bphen/Ag configuration [204].

The schematic illustration and characterization plots of inverted per-SCs fabricated by Liu et al. are given in Fig. 7 and Fig. 8, respectively.

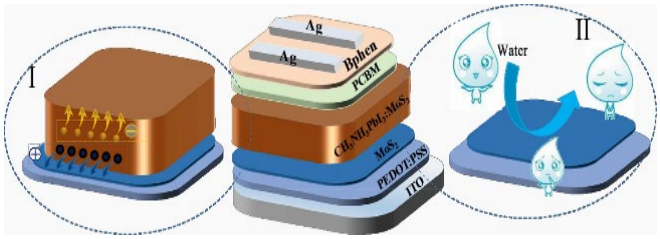

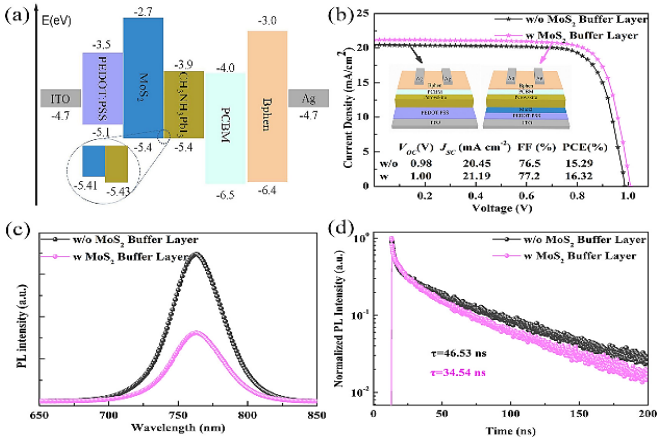

Figure 7: Schematic illustration of the PSCs with the structure of MoS_2 buffer layer and $CH_3NH_3PbI_3$:MoS_2 heterojunction. Reproduced from Ref. [204].

In another study, Liang et al. synthesized 2D nanoflakes of MoS_2 via liquid phase exfoliation to be used as BL, spin coated between spiro-OMeTAD (HTL) and perovskite ($CH_3NH_3PbI_3$) layer. They exfoliated bulk MoS_2 in two different solvents N-Methyl-2-pyrrolidone (NMP) and isopropanol (IPA), separately (Fig. 9) and compared the characteristics of both devices. Improved efficiency of 14.9% with long term stability compared to reference device was reported [205].

Figure 8: (a) Energy level diagrams of PSC device with MoS_2 buffer layer (b) J-V curves of devices and (c) Photoluminescence and (d) TRPL spectra of pure perovskite film deposited on Glass/ITO/PEDOT:PSS substrate without (black curve) and with (pink curve) MoS_2 buffer layer. Reproduced from Ref. [204].

Figure 9: Preparation of the 2D MoS_2 nanosheets. (a) Scheme of the preparation of 2D MoS_2 nanoflakes using LPE approach. (b) SEM image of exfoliated 2D MoS2 nanoflakes, and inside are exfoliated MoS_2 dispersions in an IPA (Scale bar is 500 nm). (c) Absorbance spectra of exfoliated MoS_2 nanoflakes in NMP and IPA solvents, respectively. (d) HAADF-STEM (Scale bar is 100 nm) and (e) high resolution TEM images of exfoliated MoS_2, inset in part (e) is fast Fourier transform pattern of exfoliated MoS_2 (Scale bar is 5 nm). Reproduced from Ref. [205].

6.2. $MoSe_2$ in per-SCS

Another member of the TMDCs family is $MoSe_2$ which is an in-organic compound comprising of Molybdenum and Selenium, having similar formation as that of MoS_2. The 2D-$MoSe_2$ possesses a structure similar to GR and exhibits superior electron mobilities in contrast to the 2D-MoS_2 structure. Furthermore, the monolayer structure gives a direct band gap of ~1.5 eV which makes it desirable for photovoltaic applications [206]. The first study (to best of our knowledge) on the use of $MoSe_2$ layered structure in per-SCs was reported by Chen et. al. in 2016. They fabricated a device with the structure FTO/$MoSe_2$-/perovskite/C_{60}/BCP/Ag via magnetron sputtering where $MoSe_2$ was employed as an HTL for effective hole extraction. Furthermore, they studied the domain size of the

perovskite film deposited on the HTL, as a function of annealing temperature for the $MoSe_2$ HTL. An increase in perovskite film's crystallinity was reported upon increasing the annealing temperature for the HTL film. The fabricated device exhibited a PCE of 8.23% with a J_{SC} of 14.45 $mAcm^{-2}$ [207]. Chang et. al. also utilized $MoSe_2$ as HTL for per-SC in 2020, and fabricated a device with FTO/$MoSe_2$/AL/PMMA/C_{60}/AZO/Ag structure. They also studied the crystallinity of AL as a function of annealing temperature for the HTL. A significant improvement from 10.2% to 18.0% was achieved for the optimized device, fabricated via polyethylene glycol solution. A significant increase in FF (76.12%) and reduced series resistance (17.3 Ω) was reported for the manufactured device, with a 90 nm thin $MoSe_2$ layer ass demonstrated in Fig. 10 [208].

Figure 10: (a) Schematic illustration of the multi-layered

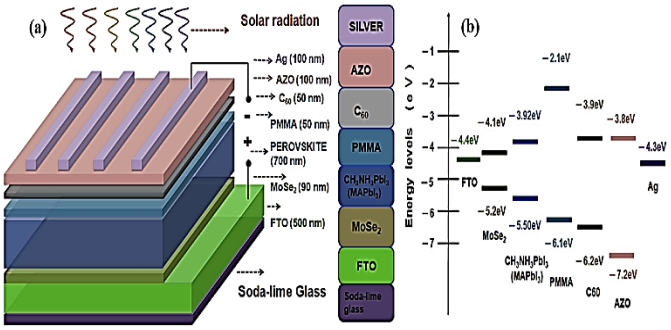

CH3NH3PbI3 solar cells with MoSe2 HTM layer and (b) energy level diagram of the Ag/AZO/C60/PMMA/MAPbI3/MoSe2/FTO multi-layered structures on glass substrate. Reproduced from Ref. [208].

In February, 2020, Huang et. al. gave further insights into the interfacial coupling and band alignments between the monolayer $MoSe_2$ and perovskite layers of SCs. They utilized $CsPbBr_3$ perovskite and $MoSe_2$ as prototypes for their computational (HSE06 and GGA-PBE) calculations, which revealed the type-II intrinsic band alignment between the two layers. They further emphasized on the interfacial deep defects sites between $CsPbBr_3$/$MoSe_2$ that could lead to enhanced PCE of per-SCs in future [209]. Liang et. al. reported the use of 2D-nanoflakes of $MoSe_2$ employed as BL for enhanced stability and better interfacial quality of per-SCs. They employed $MoSe_2$ nanoflakes between HTL (Spiro-OMeTAD) and AL ($FA_{85}MA_{15}PbI_{85}Br_{15}$) and achieved a PCE of 14.9% with significant improvement in stability as compared to reference device. The fabricated device maintained 93.1% of its initial PCE after one hour of operation which was significantly better than the reference device that retained 78.2% of its initial PCE after one hour [205]. The traditionally used TiO_2 ETL in per-SCs is although very effective but not much desirable due to high energy and time consumption in high temperature processing. On the other hand, low temperature fabrication of such ETL does not yield much desirable results in terms of uniformity and crystallinity. Zhou et. al. in April 2020, significantly improved the electron mobility of low temperature processed TiO_2 (L-TiO_2) ETL in per-SC, by incorporating $MoSe_2$ QDs in the layer. They adopted a low temperature processing route to fabricate QDs modified L-TiO_2 ETL for an all inorganic per-SC with FTO/L-TiO_2:$MoSe_2$/$CsPbBr_3$/C structure and achieved a 10.02% PCE. The enhancement in electron mobility of the ETL was attributed to the filling of trap sites in L-TiO2 by the photo-induced electrons coming from $MoSe_2$ QDs (Fig. 11). This significantly increased the charge density in the conduction band of TiO_2, hence improving the conductivity of the film [210].

Figure 11: (a) *J-V* characteristics of the device FTO/L-TiO_2:TMDCs QDs/C under dark and illumination. (b) Schematic

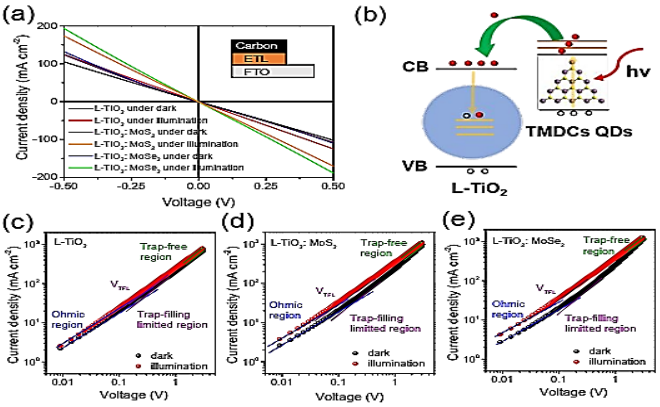

diagram of the electron transfer from TMDCs QDs to TiO_2 under illumination. Mobility and electronic traps of (c) L-TiO_2, (d) L-TiO_2:MoS_2 and (e) L-TiO_2:$MoSe_2$ under dark and illumination determined by the SCLC method. Reproduced from Ref. [210].

6.3. WS_2 in per-SCs

Tungsten disulphide (WS_2) monolayer with direct bandgap of ~2.05 eV, shows greater mobilities of carriers, better conductivity (~10^3 $\Omega^{-1}cm^{-1}$) and n-type semiconducting behaviour. Stability, less toxicity and environmental friendliness make WS_2 a potential candidate for per-SCs applications [211]. In this section, we have discussed some significant works reported on application of WS_2 in per-SCs. The first use of WS_2 in per-SCs (to best of our knowledge) was reported by Kim et. al. in 2016, where they utilized WS_2, MoS_2 and GO thin layers as replacements for PEDOT:PSS HTL. CVD approach was adopted to deposit 2D-WS2 layers on ITO and the fabricated Glass/ITO/-WS_2/Perovskite/PCBM/BCP/LiF-Al structure exhibited a PCE of 8.02%. The schematic illustration of synthetic procedure and device structure adopted by the group is given in Fig. 12 [15].

As mentioned in earlier sections, the acidic and hygroscopic nature of PEDOT:PSS HTL makes it highly undesirable in per-SCs because of reduced stability. Suitable replacements are required in this regard to improve the efficiency and stability of per-SCs. A study was reported by Huang et. al. in 2017, where PEDOT:PSS HTL was replaced by WS_2 thin layer in p-*i*-n per-SCs. They signified the importance of 1T-phase of 2D-layered TMDCs that plays the central role in improving the PCE of per-SCs. In addition to that, no post heating procedure was adopted since it causes significant decrease in 1T content of TMDCs. The fabricated device exhibited a PCE of 15% while only 12.44% of PCE was shown by the control device with PEDOT:PSS HTL. Furthermore, the stability of the device improved significantly

with 72% of initial PCE retained after 56 days of working. Whereas, the PCE of reference device dropped to zero after 35 days of operation only [212].

Figure 12: (a) Schematic of CVD synthesis for MoS2 and WS2 layers, (b) Synthesis of GO layers and (c) Schematic of per-SC

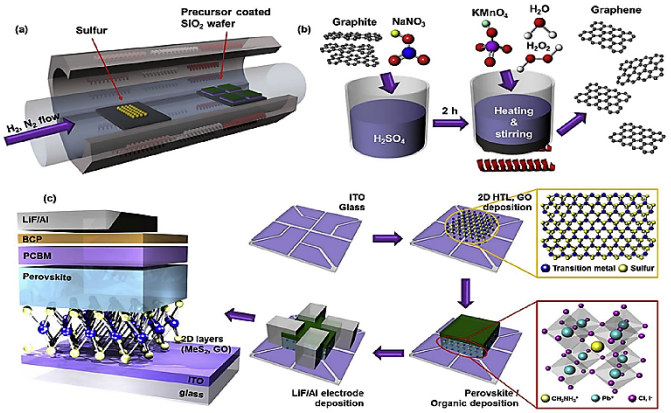

fabrication procedure and device structure. Reproduced from Ref. [211].

Another study was reported by Bayram Kilic in 2018, where WS_2 was utilized as HTL in FTO/TiO_2/Perovskite/WS_2/Ag per-SCs to achieve a PCE of 9.93% with more stability in contrast to reference device [213]. The latest study on the application of WS2 as HTL in per-SCs has been reported by Cao et. al. in 2020. The performance of per-SCs is highly dependent on interfacial as well as perovskite layer properties. These properties are much difficult to control via solution-based processes. They fabricated an inverted planar perovskite on defect free 2D nanoflakes of WS_2, used as a template for epitaxial growth. Furthermore, the cascaded alignment of energy levels and reduced recombination at the HTL/AL interface was also achieved. This resulted in a device with a PCE of 21.1% which is among the highest PCEs, attained by inverted planar per-SCs. This significant work has motivated the researchers for further exploration of 2D-LMS especially TMDCs, for efficient and stable photovoltaic devices. The device structure and epitaxial growth mechanism are demonstrated in Fig. 13 [214].

Figure 13: a) Device structure of planar inverted perovskite solar cells. b) Energy band alignment of the solar cells with WS2

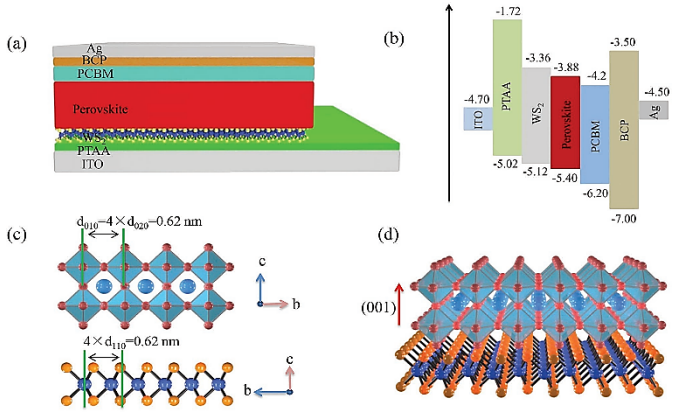

interlayer. c) Side view of crystal structure and lattice constant of perovskite and WS2. d) Schematic illustration of the epitaxial growth of perovskite film on the WS2 substrate. Reproduced from Ref. [214].

To increase the stability and performance along with low hysteresis losses in per-SC, Sobayel et. al. for the first time in 2018, investigated WS_2 as an efficient ETL through SCAPS-1D simulator. This simulation method majorly focused on the amphoteric defects as well as temperature related issues. Obtained results theoretically showed that WS_2 can be exchanged with TiO_2 as ETL in per-SCs, whereby the amphoteric defects had a great influence on its PCE which appeared as 25.7%. This estimation paved the way for TMDCs, more importantly for WS_2 as an ETL in per-SC [215]. Lead based per-SCs face the challenges of toxic lead nature as well as lower stability. Researchers have recently diverted their attention on lead free per-SCs for a sustainable future. Kumar et. al. in 2020 projected a unique structure of lead free per-SC using WS_2 as an ETL. The proposed structure was analyzed quantitatively by the simulation of solar cell capacitance. The PCE obtained by these simulations was 23% and offered lead free per-SC. The thickness of the absorber played an imperative role in optimizing the performance of the device [216]. Larger recombination rates at interfaces and electrode contacts also hinder the performance of per-SCs. Few atoms thick layers of TMDCs can overcome these challenges due to collective motion of charge carriers. Another ETL layer was developed with WS_2 in per-SC by spray pyrolysis method on ITO substrate by Malek and colleagues. The PCE was 18.21% which gained quick draining of photo electrons, rapid charge transfer at interfaces, and reducing both bulk and interfacial recombination. The performance of the device depends on thickness of WS_2 layer and showed an excellent stability but the obtained efficiency was less than the theoretically estimated value [217].

6.4. $MoTe_2$ and WSe_2 in per-SCs:

Molybdenum telluride, a compound that consists of molybdenum and telluride, is a member of TMDCs family. It can be easily crystallized into 2-D sheets and thinned down to the transparent and flexible monolayers. Among all reported TMDCs, $MoTe_2$ is least light sensitive and have potential to be useful in per-SCs. Tungsten diselenide (WSe_2) is an inorganic crystalline compound which adopts hexagonal structure. WSe_2 is very stable compound and a member of TMDCs family. As far as the applicability of per-SCs in extended devices or other circuits is concerned, very few publications have yet been reported. Significant attention is required in this area of per-SCs applicability for a more comprehensive analysis. In this regard, Jeong et. al. integrated realistic self-powered circuit by using photovoltaic cells as well as few nanometers thin $MoTe_2$ field effect transistor (FET). The n-channel few nm thin $MoTe_2$ FET was synthesized to operate glass substrate at low voltage and connected to a per-SC on another glass. Two possible operation modes (self-powered current and photo sensor) of this approach has been observed. Under visible light illumination, per-SCs in this circuit play as voltage source, providing the enough current to turn on light emitting diodes [218]. Apart from looking for replacements of PEDOT:PSS, researchers are also

searching for further modification of this HTL by functionalizing, which can significantly improve the stability and charge transfer property. Choi et al. implemented WSe_2 on PEDOT:PSS for enhancing the performance of per-SC. WSe_2 incorporation in PEDOT:PSS improved charge transport at electrode interface and photoactive layer as well as favoured the growth of perovskite crystal (Fig. 14). Consequently, an improvement in performance of solar cell having WSe_2 mediated PEDOT: PSS has shown PCE of 16.3 % [219].

Figure 14: Material preparation and device fabrication. (a) Chemical exfoliation process of WSe_2. (b) PSCs structure with P-WSe2 HTL. Reproduced from Ref. [219].

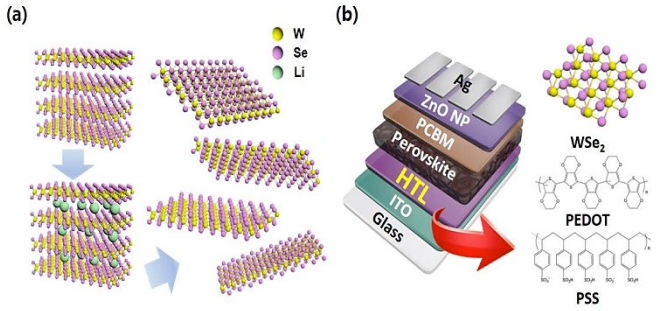

Chalcogen vacancies limit the applications of TMDCs for wide area applications as these vacancies compromise the photoconductive properties. In order to minimize these vacancies, novel techniques are required for effective performance of per-SCs. Lu et al. reported 2-D photodetector per-SC based on bilayer structure which consisted of $CH_3NH_3PbI_3$ organolead halide structure with WSe_2 monolayer. High performance of designed per-SC was achieved by perovskite functionalization and laser healing of WSe_2. After this modification, output of device was reported to be three times better as compared to pristine device [220]. These were some of the significant studies that have been reported (to our best knowledge) on carbon and TMDCs based 2D-LMs in per-SCs up to this date.

The fabrication of 2D-LMs having controlled sub-nanometre thickness from non-layered structures presents significant challenges. Though, mechanical and physical chemical deposition methods are mostly used for non-layered structures but these techniques have multiple disadvantages in the applications. Recently, liquid-metal based synthesis have emerged as an effective approach to fabricate 2D-LMs with good thickness control and better quality [221–224]. An effective technique to fabricate 2D perovskites is to exchange cations in perovskite nanocrystals with long chained alkyl groups. This is done by using long organic molecular chains which hinders the interaction of layered per-SCs using long organic molecular chains [225]. Here, self-assembly between organic chains and metal halides is compelled by the hydrogen bonding, coordination and van der Waals forces produced upon mixing. The length of the chains is crucial as it drives the reorganization to form 2D structures. Liquid metal methods which use organic alkyl ammonia molecules as long alkyl chain source are mostly used for the synthesis of per-SCs with different morphologies [226]. Nanoplatelets and nanosheets of different materials are also used for the fabrication of 2D per-solar cells due to their low cost and simplicity. Morphology and size of 2D per-SCs can be modified by controlling mass ratio and surfactant of organic cations. As compared to the traditional synthesis method, liquid metal synthesis do not apply damaging or corrosive liquids and there is no need to maintain high pressures which reduces the cost and simplify the systematic components. Liquid metal technology possess great advantages as it is capable of producing 100 Nano structure materials. The results of Al2O3, In2O3, Fe3O4 and ZnO analysis produced by the liquid metal synthesis show wide scope of their application for the fabrication of ceramics, thermal insulation, semiconductor sensors, catalysts and sorbents [227].

In 2015, 2D per-SC nanoplatelets synthesized by a liquid metal synthesis were firstly described by Tisdale and colleagues. The 2D perovskite nanoplatelets were prepared with the octylammonium bromide as long-chain ligand. 2D nanoplatelets of octylammonium bromide with varying thicknesses were attained by the slight modification of preparation technique [228]. In 2019, Wu et al. demonstrated stable and efficient perovskite devices prepared by liquid metal synthesis techniques. He used dimethylformamide as a solvent and liquid-zirconium acetate as additive. This design shows optimized film quality with lower defect states as compared to the reference device. PCE of prepared device was reported to be 20.9 % with optimum dopant concentration which maintains 98 % of its initial performance even after 1700 minutes testing under the xenon lamp. Overall, this study exhibits efficient passivating of defects and effects of crystal growth in per-SCs [229]. Producing liquid metal colloids having tailored dimensions is of great technical significance in the field of nano electronics but there is a challenge for the generation of super nano liquid metals. Yu el al. obtained ternary nano alloys by using laser irradiation in the liquids from a solid target. They studied the role of these super nano metal crystals on mediating electrons perovskite films grain boundaries. Embedding of superanano liquid metals in the per-SCs films leads to the realization of efficient cesium based per-SCs which displays an output of 21.32% [230].

A printing procedure for production of per-SCs shows encouraging application in photovoltaic commerce because of its low-cost and eco-friendly fabrication. Zhang et al. used liquid metal (Galinstan) as an interface modifier with carbon electrode. Based on high conductivity and fluidity at room temperature, it is noticed that liquid metals are superior for the improvement of hole extraction, and reserved at the interface between carbon and ZrO_2 for enhancement of contact property. Similarly, resistance for carrier transmission was decreased at perovskite interface. As optimized content, triple mesoscopic per-SCs delivers a PCE of 13.51% which involves 26% augment as compared to the ones without liquid metals [231]. Solution based metal halide per-SCs have gained a huge attraction in solar energy because of low temperature and high absorption fabrication. Boopathi et al. demonstrated droplet process of spin coating of lead halide and spray coating of methylammonium iodide for the fabrication lead iodide perovskite film. An airbrush gun was used for controlling the volume to attain a uniform, continuous and stoichiometric perovskite film. The device delivered 11.66% PCE with reproducible J_{SC}, FC and V_{OC} values [232].

Apart from the above mentioned 2D-LMS, 2D covalent organic frameworks (COFs) and metal-organic frameworks (MOFs) have also

been utilized in various functional layers of per-SCs in the past few years. A detailed discussion upon their effective applications in per-SCs has been summarized in the following section.

7. 2D COFs and MOFs in per-SCs

2D COFs and MOFs have recently acquired great attention due to their outstanding properties such as high surface area, porosity, tuneable electronic properties, excellent thermal stability, structural versatility, and relative low-cost synthesis [233]. These features make them suitable for light harvesting applications. More importantly, both frameworks have been implemented in every functional part of per-SCs including HTL, ETL and active material.

Covalent organic nanosheets (CONs) are highly desirable materials which have been recently reported by Park et al., as an interlayer in a photovoltaic device for effective alignment of energy levels between other components. This work described that different monomers may be used to resolve the challenges in the achievement of some target-HTL opto-electronic properties in the per-SCs. In contrast to prior usages of HTL layers like PEDOT:PSS, the rough surfaces of CONs were used to crystallize the photoactive layer surface and to transfer the charges towards electrodes. Moreover, this study contributed in understanding the physical contribution of every per-SC component that would be vital for shifting the ultimate research endeavors towards commercially practicable technologies [234]. Mohamed et al. carried out two types of COFs, bicarbazole coupled with 4,4',4",4"'- (ethane-1,1,2,2-tetrayl)tetranilino (Car-ETTA) and 1,3,6,8-tetrakis(4-formylphenyl)pyrene (TFPPy-ETTA). Both frameworks unveiled that greater surface area and higher crystalline nature facilitated the transfer of charge across associated interface and improved the PCE from 17.4% to 19.8%. [235]

In per-SCs, the MOF materials have been utilized as an additive for ETL, HTL, interlayer, as well as perovskite/MOF hybrids. They are the potential candidates to fabricate per-SCs with high thermal stability and efficiency. Recently, 2D MOFs are being directly utilized in various functional parts of per-SCs to enhance their performance. Chang et al. reported that a significant improvement in crystallinity and morphology of perovskite was attained by the addition of Zr-based 2D porphyrin MOF (MOF-525) as an additive. The porous MOF-525 nanocrystals introduced at the bottom of MOF/perovskite composite film which served as a scaffold to let the perovskite crystallization happen inside [236]. To increase the electron transfer between the interface of TiO_2 and perovskite, Chung et al. introduced a 2D MOF ZIF-8 layer. It not only fastened the excited electrons but also enhanced the absorption at above ~350 nm which significantly increased the PCE from 9.6% to 12.4% [237]. Later, Ryu et al. manufactured the nanocrystalline Ti-based MOF (nTi-MOF) to be employed as an efficient ETL in per-SC. The electronic character of nTi-MOF was appropriate for transfer of electrons produced in the perovskite layer upon irradiation. So, the introduction of PCBM into nTi-MOF ETLs enhanced the conductivity of the film and suppressed the direct connection between substrates and perovskite (Fig. 15). The durability was retained around ~700 bending cycles, revealing a PCE of 15.4% [238]. An updated method adopted by Zhang et al. to increase the electronic extraction and transport by utilizing 2D MOF-derived ZnO as an ETL. As a result, interface area increased between MOF-derived ZnO and per-SC which promoted carrier extraction efficiency 18.1% [239].

Figure 15: (a) Schematic of synthetic protocol for nTi-MOF (b) Structure of a per-SC introducing nTi-MOF/PCBM ETL. The magnified picture shows electron/hole transfer from perovskite towards interlayers, nTi-MOF/PCBM and spiro-OMeTAD, respectively. Reproduced from Ref. [238].

Another TiO_2 based MOF was reported by Zhao et al. for superior transportation of electron and showed PCE of 13.4% [240]. Recently, Ji et al. manufactured a champion device using polyethylenimine ethoxylated (PEIE) and tellurophene-based 2D MOF with perovskite to realize the non-destructive passivation of TiO_2. After this modification, crystallinity and morphology of perovskite film was significantly optimized, trap sites in TiO_2 layer were condensed, and transfer of electrons in device was boosted, thus finally accomplishing efficient and stable $MAPbI_3$ per-SCs with an efficiency of 22.22% [241].

To extend the application of MOF, Li et al. incorporated a 2D MOF $[In_{0.5}K(3\text{-qlc})Cl_{1.5}(H2O)_{0.5}]_{2n}$, (In10) in Spiro-OMeTAD. The inclusion of In10 oxidized Spiro-OMeTAD into Spiro-OMeTAD$^+$, and strengthened the conductivity of HTL which thus favoured the transport of charge as well as suppressed charge recombination. This modified per-SC achieved the PCE of 17% [242]. Huang et al. used 2-D lead (Pb)-based MOF and composited with Spiro-OMeTAD layer. With haloing effect, composited film showed the upshifted energy levels, smoother surface and higher hydrophobicity, as compared to a bare Spiro-OMeTAD layer. When composite layer was utilized as HTL in per-SC, the cell revealed the higher PCE (13.17%,) and moisture-resistance feather [243]. Zhou et al. introduced a MOF-derived 2D graphitic N-rich porous carbon (NPC) as an additive for HTL and verified that the incorporation of NPC can efficiently enhance the properties of HTL, supporting the extraction and migration of holes, and passivated recombination. These favourable features exhibited satisfactory PCE of 18.5% [107]. Zhang et al. constructed a bi-functional layer by introducing $(Me_2NH_2)^+$-encapsulated indium-based anionic 2D MOF (FJU-17) into hole transport material. The FJU-17 passivated cation vacancies by discharging $(Me_2NH_2)^+$ ion whereas its anionic framework was able to sustain positively charged oxidized HTM to boost mobility of holes. As a result, per-SCs exhibited better performance with PCE enhancement from 18.32% to 20.34% [244]. Almost an equivalent PCE was achieved by Zhou et al., which presented a facile method to improve the efficiency and stability per-SCs by introducing perovskite with indium-based 2D MOF $[In_{12}O(OH)_{16}(H_2O)_5(btc)_6]_n$ [245]. Recently, the role of three different supramolecular compounds of Zirconium (IV), Indium (III) and Zinc (II) with proton transfer compound, in perovskite solution, and their effect on performance of device was investigated. The MOF serving as an additive helped to form a better layer of perovskite and PCE increased from 2.9% to 5.6% (~91% improvement) after introducing of Zn metal–organic compound as an additive in per-SCs [246].

8. Interface Chemistry of 2D-LMS

It has been recognized that 2D-LMS offer tuneable heterointerfaces among dissimilar 2D layers, greater exciton mobilities, quick mass

transport, efficient excitonic separation, greater surface area, low consumption of power, and efficient tailoring of properties for the potential applications. But, inadequate knowledge of heterointerface chemistry, particularly, when unlike atoms are involved, restricts the desirable tuning and utilizing these designs in numerous applications [247,248]. Some of the most common heterointerfaces formed by the 2D-LMS have been discussed to give better understanding to young researchers as well.

The van der Waals (vdW) 2D heterostructures are raised by vdW forces like instantaneous dipole-induced-dipole, dipole-induced-dipole as well as dipole-dipole interactions, because of their interaction between edge planes [249,250]. The vdW 2D heterostructures create high anisotropy between out-of-plane and in-plane directions, and there are no requirements of matching precise processing and lattice compatibility [251–253]. Actually, the mismatch of lattices or difference of rotating angle of 2D heterostructures creates Moire´ patterns that provide assistance in tailoring the electronic and structural features of 2D-LMs [254,255]. Nonetheless, to fabricate stable 2D vdW heterostructures, the mismatching of lattice must be less than 5% (without any instability). In addition, large mismatch creates dislocations at the heterointerfaces that are favourable for ionic movement but on the same time, they can hinder the electronic properties of 2D heterostructures [256].

To understand the process of improving or introducing new properties in per-SCs, the comprehensive knowledge of physics must be known behind the heterointerface. For example, the coupling of interface between two different layers produces band aligning and tailored work function, as proposed by Anderson (heterointerface of Semiconductor–Semiconductor, S–S) or Schottky–Mott (heterointerface of Metal–Semiconductor, M–S) rules [257–259]. Exploring the heterointerface electronic band structures (S–S and M–S) is very important to discover the changes that take place at heterointerfaces. The S–S heterointerfaces band alignments are divided into 3 categories: type-I straddling gap (Fig. 16a), type-II staggered gap (Fig. 16b) and type-III broken gap (Fig. 16c) [260]. In straddling gap, VB and CB band of material S2 are present in between the material S1 bands which lead towards accumulation of h^+ and e^- and transport towards the VB and CB of material S2 [261]. The quick recombination of charge carriers in type-I shows the ability fo luminous applications (e.g, light-emitting diodes) [262]. In staggered gap, the material S1's CB and VB are higher as compared to their corresponding bands. Here, h^+ accumulation is towards material S1 and tendency of transfer of e^- is towards material S2 [263]. In type-II configuration, due to different work functions, the modulation of transition energy and charge separation at heterointerface permit extended time for the interlayer optical excitons, making it an excellent option for e^-/h^+ separator and optoelectronic devices [264,265]. The straddling gap and staggered gap heterointerfaces also suggest the opportunity to enhance the redox potential of active sites even at zero bias. In broken gap, the VB and CB of S1 are higher than CB of S2, and do not possess the zone of spatial charge as well [260]. Owing to semi-metallic response at heterointerface, the transfer of the electrons and holes in the layers of type-III 2D heterostructures produces a sturdy electric field which make them an excellent candidate for photovoltaic cells [266]. So, by designing the heterointerface carefully, based on the band alignment, new materials can be prepared for multiple applications. Furthermore, combining different semiconductors or adding different additives at a heterointerface creates a p–n junction as shown in Fig. 16d, having an induced potential difference at the interface, even when there is no external bias present [260] Moreover, the M–S heterointerfaces are fashioned among n- or p-type semiconductors, semi-metals and metals, where e^- flows and electronic interaction is prejudiced by Schottky effect in heterointerfaces [267,268]. A change in electron density as well as in Fermi level occur due to e^- flow which enhances the M–S heterointerface chemical reactivity (Fig. 16 e and f) [269,270].

Figure 16: (a–f) Schematic illustration of electronic band structures of typical S–S heterointerfaces and M–S heterointerfaces. Reproduced from Ref. [264].

2D-LMS form electronic coupling and tune the e^- transfer at heterointerfaces by a suitable combination of different materials [260,271]. Similarly, the strength of coupling at heterointerfaces can affect the charge transfer excitons dynamics and offer PL features to 2D-LMS. Interestingly, PL characteristics as well as exciton dynamics can be further modified by introducing dielectric layers at the heterointerface [247]. The adsorption energies can be tuned with vdW interactions at the heterointerface which decreases diffusion potential for the ions, permitting multilayer ions adsorption at very low expansion for the cycling stability [249]. The weak vdW connections of basal planes offer dynamically stablized 2D heterostructures having changeable interlayer spacing for quick ion dispersion, even for Na^+ and K^+ ions having larger ionic radius and polarized ions like Mg^{2+} [272,273]. These properties can be modified for per-SCs with various functional groups presence and through stacking order of the distinct layers. In addition to the band modulation, managing the values of interlayer distance also lift e^- and ionic transfer, leading to the enhanced electrochemical properties per-SCs [253,274]. The greater interlayer spacing offers direct penetration of electrolyte at the heterointerface; therefore, charges only need to diffuse a few angstroms (Å) distance [275]. This separation may be further modified in 2D heterostructures and varying spacing values are attained in contrast to bare 2D-LMs that can help in realizing more advanced per-SCs [247]. In summary, vdW 2D heterostructures offer great opportunity in selecting suitable material combinations for yielding interface-induced desirable chemical as well as physical features. The engineering of 2D heterointerface revealed that 2D heterostructures exhibit superior performance in per-SCs in contrast to individual counterparts. Moreover, there are some restrictions which strongly suggest to construct the 2D heterointerfaces with strong chemical bonds and fast charge transport mechanism to get more stable structures for per-SCs.

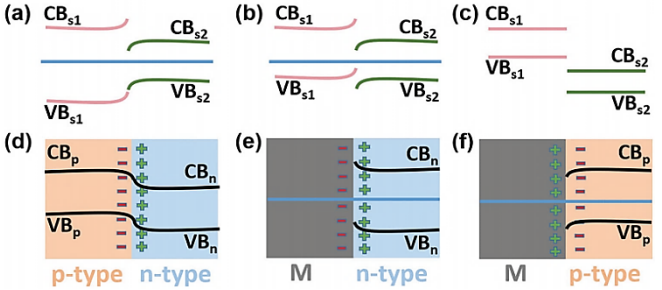

The demand of highly stable and tuneable characteristics of heterointerfaces for improved performance of per-SCs gave an idea for a novel type of 2D heterostructures that are covalently bonded. The covalent interactions can take place with the help of a linker or directly between two different materials such as EDC and Sonogashira couplings for growing a stabilized structure. These connections strongly hold the dissimilar materials together, under severe circumstances, and also provide straight highways between dissimilar materials for the ultrafast movement of charges utilizing covalent bonds [276]. Usually, there are no dangling bonds present in the 2D-LMS or they do not possess clean interfaces, hence they need linkers to grow covalently bonded 2D heterostructures. Moreover, covalent heterostructures with linker support need not to fulfil the requirement of lattice matching, therefore offer huge flexibility in selecting combination of different materials for assembling the 2D heterostructures. These amendments may increase the performance of per-SCs and energy storage devices as well [247]. Additionally, cross-linking also generates planarity which plays its role in an efficient charge transfer in 2-D heterostructures, owing to orbital overlapping [277]. The covalent linkages assist in enhancing the charge transfer between heterointerfaces and provide a larger surface area for increased photochemical reactions in per-SCs [278]. In addition, simply tuning the movement of charges and functionalization of 2D-LMs to build covalently bonded 2D heterostructures generates defects that can further modify their properties and ultimately improve the performance of solar cells.

9. Summary and Future Outlooks

Remarkable progress in only few years have significantly enabled per-SCs to approach the standards of other functional silicon-based photovoltaics. However, some challenges still prevail, regarding the long-term stability of these perovskite devices which hinder their commercialization and upscaling. Stable and inexpensive materials need to be explored for enhancement of per-SCs efficiency and stability. In this regard, 2D-LMs have recently emerged as a competitive class of materials that can open potential pathways toward the sustainable future of SC-technology. In this review, we have summarized various applications of various 2D-LMs in per-SCs. Owing to their tuneable properties and structures, these 2D-LMs can be effectively employed in all functional layers of per-SCs to boost the overall performance. Apart from significant reduction in net cost, 2D-LMS also offer homogeneous films with well-defined interfaces that can be engineered effectively. Regardless of such overwhelming advantages, further efforts still need to be made for promoting their applications in per-SCs.

The correlation between the synthesis procedures and materials performance need to be addressed more vigorously. The fast nucleation rates involved in one-step synthesis methods result in poor crystallization of active layers while the slow nucleation rates in two-step fabrication routes generate relatively large crystals with poor performance. There is an ample need to further explore these synthesis techniques to get simultaneously achieve fast and well-ordered nucleation. In addition to that, we have noticed that spin coating is the most adopted technique to deposit 2D-LMs films on various substrates. Although, this technique offer several advantages of low cost, easy availability and convenience, the layers deposited by this method do not fully cover the underlying layers. The incomplete coverage results in generation of voids in large quantities and the performance of the device is heavily compromised. One solution can be to increase the number of layers deposited on the substrates but this will cause roughness and poor transparency of films, consequently increasing the series resistance in the devices. Hence, developing more efficient deposition procedures to introduce 2D-LMs in per-SCs is of great importance.

Apart from improved efficiencies in per-SCs, 2D-LMs have drastically boosted the stability of these devices as well. Further research in coming years will definitely address thie significant issue of device stability by employing 2D-LMs in per-SCs. Efforts are being made to effectively functionalize these 2D materials with appropriate compounds to boost their hydrophobic nature and thermal stability. Hetero-doping of various 2D-LMs such as TMDCs and MXenes based HTLS with proper functionalizing can prove to be highly effective in this regard. Encapsulating the device with hydrophobic HTLs ans direct introduction of hydrophobic elements in the device structure can significantly improve the stability against moist conditions.

Carbon-based nanomaterials, especially 2D-LMs have been extensively explored for their applications in SC technology in past few years because of their extensive stability and cost effectiveness. Moreover, their hydrophobic nature (water repellent) has significantly improved the stability of devices in moist environment, which is extremely important. However, we still believe that more studies are needed on combined effect of humidity, light and high temperature on stability of C-LMs based photovoltaic devices. Although, C-LMs seem to have reached a level of saturation in their applicability in SC technology, we expect that more reports will be published on their improved applications in third generation per-SCs, in near future as well. Furthermore, newly developed GR-derivatives such as GY and GDY have emerged as promising candidates to replace GR, GO and RGO in all functional layers of per-SCs. They present homogeneous distribution of pores, great flexibility and unique electronic behaviour in contrast to other GR derivatives. We believe that further exploration of these materials will prove highly productive in pushing the PCE of per-SCs beyond 25%.

Furthermore, an alternate for C-LMs based SCs that have emerged quite recently is a new class of materials named as TMDCs, which have shown extraordinary potential as a replacement of C-LMs in SC technology. TMDCs have shown high catalytic, absorptive and stable properties and are relatively inexpensive as well. This has intrigued many researchers to develop modern and cost-effective synthetic approaches to fabricate highly effective and stable TMDCs. Micromechanical cleavage synthesis that offer nanosheets of high quality is one of the examples but it is not much suitable for large or commercial scale fabrication. Other synthetic methods including CVD, electrochemical exfoliation and liquid exfoliation have been reported with reliable results as well. The

ultrasonic spray pyrolysis technique has shown significant effects on the performance of fabricated TMDCs in per-SCs. Furthermore, the charge transfer properties of TMDCs such as MoS_2 can be effectively enhanced by functionalizing with PAS. Furthermore, compositing TMDCs with organic HTLS such as PCBM, P3HT and PEDOT:PSS has proven to be an effective approach to boost their PV performance in per-SCs. Moreover, studies have revealed that utilizing 1T-rich phases of TMDCs including MoS_2 and WS_2 as HTLs result in higher PCEs as compared to other phases. TMDCs based ETLs in per-SCs have shown promising results as well, since MoS_2, $MoSe_2$ and WS_2 offer swift vertical charge transport and uniform layers with lesser dangling bonds. Additionally, these 2D-LMs have been composited with various metal oxides such as ZnO and TiO_2 to enhance their electron extraction abilities in per-SCs. In order to improve the stability of per-SCs, these 2D TMDCs have also been used as buffer layers between the functional parts of the SC to prevent device degradation. Some recently emerged TMDCs based 2D-LMS such as $MoTe_2$, WSe_2 and $PtSe_2$ can prove to be potential candidates for improved charge transport behaviours and they should be further explored in various parts of per-SCs. Nevertheless, we believe that there is plenty of margin available for exploring these 2D-LMs in order to further enhance the stability and efficiency of per-SCs.

Apart from the traditional 2D-LMs utilized in per-SCs, 2D MOFs and COFs have gained significant attention in the recent years. High PCEs of up to 20% have already been reported, owing to the unique properties of these novel 2D structures. With proper synthesis and tuning, 2D MOFs and COFs could effective replace costly materials and help in realizing cost effective and flexible per-SCs with improved efficiencies and stabilities. We expect to see more intimate research reports on their use in per-SCs in the near future.

Since, abundant amount of work has been reported on carbon-based materials in recent years, we have focused more on TMDCs and their applications in per-SCs. Various applications of 2D C-LMs and TMDCs based LMs in all functional layers of per-SCs were briefly discussed for reader's convenience. Although, number of works have been reported on the use of TMDCs-LMs in organic, dye sensitized and silicon based SCs, only limited studies have been reported on their application in per-SCs. Furthermore, we have found no significant work on use of MoS_2 based electrodes in per-SCs and we expect to see yielding reports on their use as counter electrodes in near future. As far as C-LMs are concerned, we believe that there is still room to develop C-LMs based CE with lesser resistance to improve the PCE of per-SCs. Moreover, frequent studies on upscaling and commercialization of C-LMS based per-SCs is encouraging researchers to look for more adequate synthesis approaches and compact results are expected in coming years.

In conclusion, our review will help and encourage researchers to further explore 2D-LMs based on carbon and TMDCs to improve stability and performance of these promising third generation, in future. It will provide researcher with compact and resourceful information on above mentioned materials and their application in various functional parts of per-SCs. We believe that 2D-LMs are a promising pathway for sustainable solar based energy production to meet our ever-growing demands.

Author Contributions

We strongly encourage authors to include author contributions and recommend using CRediT for standardised contribution descriptions. Please refer to our general author guidelines for more information about authorship.

Conflicts of interest

There are no conflicts to declare.

Acknowledgements

The acknowledgements come at the end of an article after the conclusions and before the notes and references.

References

1 N. J. Jeon, J. H. Noh, W. S. Yang, Y. C. Kim, S. Ryu, J. Seo and S. Il Seok, *Nat. 2015 5177535*, 2015, **517**, 476–480.

2 S. Yang, W. Fu, Z. Zhang, H. Chen and C. Z. Li, *J. Mater. Chem. A*, 2017, 5, 11462–11482.

3 B. O'Regan and M. Grätzel, *Nature*, 1991, **353**, 737–740.

4 G. Yu, J. Gao, J. C. Hummelen, F. Wudl and A. J. Heeger, *Science (80-.).*, 1995, **270**, 1789.

5 C. W. Tang, *Appl. Phys. Lett.*, 1986, **48**, 183–185.

6 J. Xu, Y. Chen and L. Dai, *Nat. Commun.*, 2015, **6**, 1–7.

7 F. Gao, Y. Zhao, X. Zhang and J. You, *Adv. Energy Mater.*, 2020, **10**, 1902650.

8 D. W. DeQuilettes, S. M. Vorpahl, S. D. Stranks, H. Nagaoka, G. E. Eperon, M. E. Ziffer, H. J. Snaith and D. S. Ginger, *Science (80-.).*, 2015, **348**, 683–686.

9 C. Wehrenfennig, G. E. Eperon, M. B. Johnston, H. J. Snaith and L. M. Herz, *Adv. Mater.*, 2014, **26**, 1584–1589.

10 S. D. Stranks, G. E. Eperon, G. Grancini, C. Menelaou, M. J. P. Alcocer, T. Leijtens, L. M. Herz, A. Petrozza and H. J. Snaith, *Science (80-.).*, 2013, **342**, 341–344.

11 G. Xing, N. Mathews, S. Sun, S. S. Lim, Y. M. Lam, M. Graẗzel, S. Mhaisalkar and T. C. Sum, *Science (80-.).*, 2013, **342**, 344–347.

12 Q. Dong, Y. Fang, Y. Shao, P. Mulligan, J. Qiu, L. Cao and J. Huang, *Science (80-.).*, 2015, **347**, 967–970.

13 Z. Wang, Z. Shi, T. Li, Y. Chen and W. Huang, *Angew. Chemie Int. Ed.*, 2017, **56**, 1190–1212.

14 F. Giustino and H. J. Snaith, *ACS Energy Lett.*, 2016, 1, 1233–1240.

15 Y. G. Kim, K. C. Kwon, Q. Van Le, K. Hong, H. W. Jang and S. Y. Kim, *J. Power Sources*, 2016, **319**, 1–8.

16 S. Z. Butler, S. M. Hollen, L. Cao, Y. Cui, J. A. Gupta, H. R. Gutiérrez, T. F. Heinz, S. S. Hong, J. Huang, A. F. Ismach, E. Johnston-Halperin, M. Kuno, V. V Plashnitsa, R. D. Robinson, R. S. Ruoff, S. Salahuddin, J. Shan, L. Shi, M. G. Spencer, M. Terrones, W. Windl and J. E. Goldberger, *ACS Nano*, 2013, 7, 2898–2926.

17 H. Zhang, *Chem. Rev.*, 2018, 118, 6089–6090.

18 D. Jariwala, V. K. Sangwan, L. J. Lauhon, T. J. Marks and M. C. Hersam, *ACS Nano*, 2014, 8, 1102–1120.

19 X. Duan, C. Wang, A. Pan, R. Yu and X. Duan, *Chem. Soc. Rev.*, 2015, 44, 8859–8876.

20 L. Ci, L. Song, C. Jin, D. Jariwala, D. Wu, Y. Li, A. Srivastava, Z. F. Wang, K. Storr, L. Balicas, F. Liu and P. M. Ajayan, *Nat. Mater.*, 2010, **9**, 430–435.

21 A. Pakdel, C. Zhi, Y. Bando and D. Golberg, *Mater. Today*, 2012, 15, 256–265.

22 P. Vogt, P. De Padova, C. Quaresima, J. Avila, E. Frantzeskakis, M. C. Asensio, A. Resta, B. Ealet and G. Le Lay, *Phys. Rev. Lett.*, 2012, **108**, 155501.

23 H. Zhang, H. M. Cheng and P. Ye, *Chem. Soc. Rev.*, 2018, 47, 6009–6012.

24 C. Tan, X. Cao, X. J. Wu, Q. He, J. Yang, X. Zhang, J. Chen, W. Zhao, S. Han, G. H. Nam, M. Sindoro and H. Zhang, *Chem. Rev.*, 2017, 117, 6225–6331.

25 H. Tributsch and J. C. Bennett, *J. Electroanal. Chem.*, 1977, **81**, 97–111.

26 K. S. Novoselov, V. I. Fal'Ko, L. Colombo, P. R. Gellert, M. G. Schwab and K. Kim, *Nature*, 2012, 490, 192–200.

27 R. Fivaz and E. Mooser, *Phys. Rev.*, 1967, **163**, 743–755.

28 H. Wang, F. Liu, W. Fu, Z. Fang, W. Zhou and Z. Liu, *Nanoscale*, 2014, 6, 12250–12272.

29 Y. Zhu, S. Murali, W. Cai, X. Li, J. W. Suk, J. R. Potts and R. S. Ruoff, *Adv. Mater.*, 2010, **22**, 3906–3924.

30 H. Kim, C. M. Gilmore, A. Piqué, J. S. Horwitz, H. Mattoussi, H. Murata, Z. H. Kafafi and D. B. Chrisey, *J. Appl. Phys.*, 1999, **86**, 6451–6461.

31 J. Gusakova, X. Wang, L. L. Shiau, A. Krivosheeva, V. Shaposhnikov, V. Borisenko, V. Gusakov and B. K. Tay, *Phys. status solidi*, 2017, **214**, 1700218.

32 M. Velický and P. S. Toth, *Appl. Mater. Today*, 2017, 8, 68–103.

33 M. Pumera, Z. Sofer and A. Ambrosi, *J. Mater. Chem. A*, 2014, **2**, 8981–8987.

34 S. N. Habisreutinger, D. P. McMeekin, H. J. Snaith and R. J. Nicholas, *APL Mater.*, 2016, **4**, 91503.

35 M. Saliba, T. Matsui, J. Y. Seo, K. Domanski, J. P. Correa-Baena, M. K. Nazeeruddin, S. M. Zakeeruddin, W. Tress, A. Abate, A. Hagfeldt and M. Grätzel, *Energy Environ. Sci.*, 2016, **9**, 1989–1997.

36 H. Tsai, W. Nie, J. C. Blancon, C. C. Stoumpos, R. Asadpour, B. Harutyunyan, A. J. Neukirch, R. Verduzco, J. J. Crochet, S. Tretiak, L. Pedesseau, J. Even, M. A. Alam, G. Gupta, J. Lou, P. M. Ajayan, M. J. Bedzyk, M. G. Kanatzidis and A. D. Mohite, *Nature*, 2016, **536**, 312–317.

37 H. Chen and S. Yang, *J. Mater. Res.*, 2017, **32**, 3011–3020.

38 M. C. dos Santos, M. C. Maynart, L. R. Aveiro, E. C. da Paz and V. dos Santos Pinheiro, *Carbon-Based Materials: Recent Advances, Challenges, and Perspectives*, Elsevier Ltd., 2017.

39 M. Bernardi, M. Palummo and J. C. Grossman, *Nano Lett.*, 2013, **13**, 3664–3670.

40 M. Shanmugam, T. Bansal, C. A. Durcan and B. Yu, *Appl. Phys. Lett.*, 2012, **101**, 263902.

41 X. Huang, Z. Yin, S. Wu, X. Qi, Q. He, Q. Zhang, Q. Yan, F. Boey and H. Zhang, *Small*, 2011, **7**, 1876–1902.

42 S. Bertolazzi, J. Brivio and A. Kis, *ACS Nano*, 2011, **5**, 9703–9709.

43 Z. M. Beiley and M. D. McGehee, *Energy Environ. Sci.*, 2012, **5**, 9173–9179.

44 M. Alzaid, *Int. J. Energy Res.*, 2021, **45**, 12598–12613.

45 M. Saliba, T. Matsui, K. Domanski, J. Y. Seo, A. Ummadisingu, S. M. Zakeeruddin, J. P. Correa-Baena, W. R. Tress, A. Abate, A. Hagfeldt and M. Grätzel, *Science (80-.).*, 2016, **354**, 206–209.

46 J. P. Correa Baena, L. Steier, W. Tress, M. Saliba, S. Neutzner, T. Matsui, F. Giordano, T. J. Jacobsson, A. R. Srimath Kandada, S. M. Zakeeruddin, A. Petrozza, A. Abate, M. K. Nazeeruddin, M. Grätzel and A. Hagfeldt, *Energy Environ. Sci.*, 2015, **8**, 2928–2934.

47 K. A. Bush, C. D. Bailie, Y. Chen, A. R. Bowring, W. Wang, W. Ma, T. Leijtens, F. Moghadam and M. D. McGehee, *Adv. Mater.*, 2016, **28**, 3937–3943.

48 K. Domanski, J. P. Correa-Baena, N. Mine, M. K. Nazeeruddin, A. Abate, M. Saliba, W. Tress, A. Hagfeldt and M. Grätzel, *ACS Nano*, 2016, **10**, 6306–6314.

49 S. Gholipour, J.-P. Correa-Baena, K. Domanski, T. Matsui, L. Steier, F. Giordano, F. Tajabadi, W. Tress, M. Saliba, A. Abate, A. Morteza Ali, N. Taghavinia, M. Grätzel and A. Hagfeldt, *Adv. Energy Mater.*, 2016, **6**, 1601116.

50 K. Aitola, K. Domanski, J.-P. Correa-Baena, K. Sveinbjörnsson, M. Saliba, A. Abate, M. Grätzel, E. Kauppinen, E. M. J. Johansson, W. Tress, A. Hagfeldt and G. Boschloo, *Adv. Mater.*, 2017, **29**, 1606398.

51 A. Mei, X. Li, L. Liu, Z. Ku, T. Liu, Y. Rong, M. Xu, M. Hu, J. Chen, Y. Yang, M. Grätzel and H. Han, *Science (80-.).*, 2014,

345, 295–298.

52 G. Niu, W. Li, F. Meng, L. Wang, H. Dong and Y. Qiu, *J. Mater. Chem. A*, 2014, **2**, 705–710.

53 J. A. Christians, P. A. Miranda Herrera and P. V Kamat, *J. Am. Chem. Soc.*, 2015, **137**, 1530–1538.

54 K. A. Bush, A. F. Palmstrom, Z. J. Yu, M. Boccard, R. Cheacharoen, J. P. Mailoa, D. P. McMeekin, R. L. Z. Hoye, C. D. Bailie, T. Leijtens, I. M. Peters, M. C. Minichetti, N. Rolston, R. Prasanna, S. Sofia, D. Harwood, W. Ma, F. Moghadam, H. J. Snaith, T. Buonassisi, Z. C. Holman, S. F. Bent and M. D. McGehee, *Nat. Energy*, 2017, **2**, 1–7.

55 Q. Tai, P. You, H. Sang, Z. Liu, C. Hu, H. L. W. Chan and F. Yan, *Nat. Commun.*, 2016, **7**, 1–8.

56 J. Idígoras, F. J. Aparicio, L. Contreras-Bernal, S. Ramos-Terrón, M. Alcaire, J. R. Sánchez-Valencia, A. Borras, Á. Barranco and J. A. Anta, *ACS Appl. Mater. Interfaces*, 2018, **10**, 11587–11594.

57 Z. Li, C. Xiao, Y. Yang, S. P. Harvey, D. H. Kim, J. A. Christians, M. Yang, P. Schulz, S. U. Nanayakkara, C. S. Jiang, J. M. Luther, J. J. Berry, M. C. Beard, M. M. Al-Jassim and K. Zhu, *Energy Environ. Sci.*, 2017, **10**, 1234–1242.

58 T. Leijtens, G. E. Eperon, S. Pathak, A. Abate, M. M. Lee and H. J. Snaith, *Nat. Commun.*, 2013, **4**, 1–8.

59 B. Roose, J. P. C. Baena, K. C. Gödel, M. Graetzel, A. Hagfeldt, U. Steiner and A. Abate, *Nano Energy*, 2016, **30**, 517–522.

60 F. Bella, G. Griffini, J. P. Correa-Baena, G. Saracco, M. Grätzel, A. Hagfeldt, S. Turri and C. Gerbaldi, *Science (80-.).*, 2016, **354**, 203–206.

61 N. J. Jeon, J. H. Noh, Y. C. Kim, W. S. Yang, S. Ryu and S. Il Seok, *Nat. Mater.*, 2014, **13**, 897–903.

62 K. Domanski, B. Roose, T. Matsui, M. Saliba, S. H. Turren-Cruz, J. P. Correa-Baena, C. R. Carmona, G. Richardson, J. M. Foster, F. De Angelis, J. M. Ball, A. Petrozza, N. Mine, M. K. Nazeeruddin, W. Tress, M. Grätzel, U. Steiner, A. Hagfeldt and A. Abate, *Energy Environ. Sci.*, 2017, **10**, 604–613.

63 M. Bag, L. A. Renna, R. Y. Adhikari, S. Karak, F. Liu, P. M. Lahti, T. P. Russell, M. T. Tuominen and D. Venkataraman, *J. Am. Chem. Soc.*, 2015, **137**, 13130–13137.

64 M. Becker and M. Wark, *Zeitschrift für Naturforsch. A*, 2019, **74**, 655–663.

65 Y. Zhou, O. S. Game, S. Pang and N. P. Padture, *J. Phys. Chem. Lett.*, 2015, **6**, 4827–4839.

66 M. Xiao, F. Huang, W. Huang, Y. Dkhissi, Y. Zhu, J. Etheridge, A. Gray-Weale, U. Bach, Y.-B. Cheng and L. Spiccia, *Angew. Chemie Int. Ed.*, 2014, **53**, 9898–9903.

67 D. T. Moore, H. Sai, K. W. Tan, D.-M. Smilgies, W. Zhang, H. J. Snaith, U. Wiesner and L. A. Estroff, *J. Am. Chem. Soc.*, 2015, **137**, 2350–2358.

68 D. T. Moore, H. Sai, K. W. Tan, L. A. Estroff and U. Wiesner, *APL Mater.*, 2014, **2**, 81802.

69 R. Munir, A. D. Sheikh, M. Abdelsamie, H. Hu, L. Yu, K. Zhao, T. Kim, O. El Tall, R. Li, D.-M. Smilgies and A. Amassian, *Adv. Mater.*, 2017, **29**, 1604113.

70 J. Burschka, N. Pellet, S.-J. Moon, R. Humphry-Baker, P. Gao, M. K. Nazeeruddin and M. Grätzel, *Nat. 2013 4997458*, 2013, **499**, 316–319.

71 B. J. Foley, Justin Girard, B. A. Sorenson, A. Z. Chen, J. S. Niezgoda, M. R. Alpert, A. F. Harper, Detlef-M. Smilgies, Paulette Clancy, W. A. Saidi and J. J. Choi, *J. Mater. Chem. A*, 2016, **5**, 113–123.

72 J. Schlipf, P. Docampo, C. J. Schaffer, V. Körstgens, L. Bießmann, F. Hanusch, N. Giesbrecht, S. Bernstorff, T. Bein and P. Müller-Buschbaum, *J. Phys. Chem. Lett.*, 2015, **6**, 1265–1269.

73 C. Roldán-Carmona, O. Malinkiewicz, A. Soriano, G. M. Espallargas, A. Garcia, P. Reinecke, T. Kroyer, M. I. Dar, M. K. Nazeeruddin and H. J. Bolink, *Energy Environ. Sci.*, 2014, **7**, 994–997.

74 V. M. Bannur, *https://doi.org/10.1142/S0217751X14500560*, , DOI:10.1142/S0217751X14500560.

75 R. P.-A. de l'institut H. Poincaré and U. 1935, *numdam.org*.

76 N. D. Mermin, *Phys. Rev.*, 1968, **176**, 250.

77 K. S. Novoselov, A. K. Geim, S. V Morozov, D. Jiang, Y. Zhang, S. V Dubonos, I. V Grigorieva and A. A. Firsov, *Science (80-.).*, 2004, **306**, 666–669.

78 V. Nicolosi, M. Chhowalla, M. G. Kanatzidis, M. S. Strano and J. N. Coleman, *Science (80-.).*, , DOI:10.1126/SCIENCE.1226419.

79 K. Ramasamy, H. Sims, W. H. Butler and A. Gupta, *J. Am. Chem. Soc.*, 2014, **136**, 1587–1598.

80 Z. Cai, B. Liu, X. Zou and H.-M. Cheng, *Chem. Rev.*, 2018, **118**, 6091–6133.

81 H. Li, Y. Li, A. Aljarb, Y. Shi and L.-J. Li, *Chem. Rev.*, 2017, **118**, 6134–6150.

82 J. H. Han, M. Kwak, Y. Kim and J. Cheon, *Chem. Rev.*, 2018, **118**, 6151–6188.

83 R. Dong, T. Zhang and X. Feng, *Chem. Rev.*, 2018, **118**, 6189–6325.

84 M. Zeng, Y. Xiao, J. Liu, K. Yang and L. Fu, *Chem. Rev.*, 2018, **118**, 6236–6296.

85 H. Jin, C. Guo, X. Liu, J. Liu, A. Vasileff, Y. Jiao, Y. Zheng and S.-Z. Qiao, *Chem. Rev.*, 2018, **118**, 6337–6408.

86 G. H. Han, D. L. Duong, D. H. Keum, S. J. Yun and Y. H. Lee, *Chem. Rev.*, 2018, **118**, 6297–6336.

87 Y. Chen, Z. Fan, Z. Zhang, W. Niu, C. Li, N. Yang, B. Chen and

H. Zhang, *Chem. Rev.*, 2018, **118**, 6409–6455.

88 Z. Wu, T. Song and B. Sun, *ChemNanoMat*, 2017, **3**, 75–88.

89 M. Hadadian, J. H. Smått and J. P. Correa-Baena, *Energy Environ. Sci.*, 2020, 13, 1377–1407.

90 X. Wan, Y. Huang and Y. Chen, *Acc. Chem. Res.*, 2012, **45**, 598–607.

91 E. Liang Lim, C. Chin Yap, M. Hafizuddin Hj Jumali, M. Asri Mat Teridi and C. Hoong Teh, *Nano-Micro Lett.*, , DOI:10.1007/s40820-017-0182-0.

92 M. Batmunkh, C. J. Shearer, M. J. Biggs and J. G. Shapter, *J. Mater. Chem. A*, 2015, **3**, 9020–9031.

93 H. S. Kim, C. R. Lee, J. H. Im, K. B. Lee, T. Moehl, A. Marchioro, S. J. Moon, R. Humphry-Baker, J. H. Yum, J. E. Moser, M. Grätzel and N. G. Park, *Sci. Rep.*, 2012, **2**, 1–7.

94 T. Liu, D. Kim, H. Han, A. R. Bin Mohd Yusoff and J. Jang, *Nanoscale*, 2015, **7**, 10708–10718.

95 Q. D. Yang, J. Li, Y. Cheng, H. W. Li, Z. Guan, B. Yu and S. W. Tsang, *J. Mater. Chem. A*, 2017, **5**, 9852–9858.

96 E. S. Choi, Y. J. Jeon, S. S. Kim, T. W. Kim, Y. J. Noh, S. N. Kwon and S. I. Na, *Appl. Phys. Lett.*, 2015, **107**, 23301.

97 E. Jokar, Z. Y. Huang, S. Narra, C.-Y. Wang, V. Kattoor, C.-C. Chung and E. W.-G. Diau, *Adv. Energy Mater.*, 2018, **8**, 1701640.

98 J. S. Yeo, C. H. Lee, D. Jang, S. Lee, S. M. Jo, H. I. Joh and D. Y. Kim, *Nano Energy*, 2016, **30**, 667–676.

99 A. L. Palma, L. Cinà, S. Pescetelli, A. Agresti, M. Raggio, R. Paolesse, F. Bonaccorso and A. Di Carlo, *Nano Energy*, 2016, **22**, 349–360.

100 Xiaoru Wen, Jiamin Wu, Di Gao and Changjian Lin, *J. Mater. Chem. A*, 2016, **4**, 13482–13487.

101 K. T. Cho, G. Grancini, Y. Lee, D. Konios, S. Paek, E. Kymakis and M. K. Nazeeruddin, *ChemSusChem*, 2016, **9**, 3040–3044.

102 J.-J. Park, M. Lee, Y. Kim and D.-Y. Kim, *Sol. RRL*, 2021, **5**, 2100087.

103 Q. Q. Chu, B. Ding, J. Peng, H. Shen, X. Li, Y. Liu, C. X. Li, C. J. Li, G. J. Yang, T. P. White and K. R. Catchpole, *J. Mater. Sci. Technol.*, 2019, **35**, 987–993.

104 B. Xie, Y. Zhang, Y. Li, W. Chen, X. Hu and S. Zhang, *J. Mater. Sci. Mater. Electron. 2020 318*, 2020, **31**, 6248–6254.

105 C. Redondo-Obispo, T. S. Ripolles, S. Cortijo-Campos, A. L. Álvarez, E. Climent-Pascual, A. de Andrés and C. Coya, *Mater. Des.*, 2020, **191**, 108587.

106 M. Habib, M. Feteha, M. Soliman, A. A. Motagaly, S. El-Sheikh and S. Ebrahim, *J. Mater. Sci. Mater. Electron. 2020 3121*, 2020, **31**, 18870–18882.

107 X. Zhou, L. Qiu, R. Fan, A. Wang, H. Ye, C. Tian, S. Hao and Y. Yang, *Sol. RRL*, 2020, **4**, 1900380.

108 A. L. Palma, L. Cinà, S. Pescetelli, A. Agresti, M. Raggio, R. Paolesse, F. Bonaccorso and A. Di Carlo, *Nano Energy*, 2016, **22**, 349–360.

109 Z. Wu, S. Bai, J. Xiang, Z. Yuan, Y. Yang, W. Cui, X. Gao, Z. Liu, Y. Jin and B. Sun, *Nanoscale*, 2014, **6**, 10505–10510.

110 D. Li, J. Cui, H. Li, D. Huang, M. Wang and Y. Shen, *Sol. Energy*, 2016, **131**, 176–182.

111 J. S. Yeo, R. Kang, S. Lee, Y. J. Jeon, N. S. Myoung, C. L. Lee, D. Y. Kim, J. M. Yun, Y. H. Seo, S. S. Kim and S. I. Na, *Nano Energy*, 2015, **12**, 96–104.

112 P. You, Z. Liu, Q. Tai, S. Liu and F. Yan, *Adv. Mater.*, 2015, **27**, 3632–3638.

113 Z. Liu, P. You, C. Xie, G. Tang and F. Yan, *Nano Energy*, 2016, **28**, 151–157.

114 H. Sung, N. Ahn, M. S. Jang, J.-K. Lee, H. Yoon, N.-G. Park and M. Choi, *Adv. Energy Mater.*, 2016, **6**, 1501873.

115 K. Yan, Z. Wei, J. Li, H. Chen, Y. Yi, X. Zheng, X. Long, Z. Wang, J. Wang, J. Xu and S. Yang, *Small*, 2015, **11**, 2269–2274.

116 D. H. Shin, J. M. Kim, S. H. Shin and S. H. Choi, *Dye. Pigment.*, 2019, **170**, 107630.

117 H. Bian, Q. Wang, S. Yang, C. Yan, H. Wang, L. Liang, Z. Jin, G. Wang and S. Liu, *J. Mater. Chem. A*, 2019, **7**, 5740–5747.

118 I. Jeon, J. Yoon, N. Ahn, M. Atwa, C. Delacou, A. Anisimov, E. I. Kauppinen, M. Choi, S. Maruyama and Y. Matsuo, *J. Phys. Chem. Lett.*, 2017, **8**, 5395–5401.

119 J. H. Heo, D. H. Shin, S. Kim, M. H. Jang, M. H. Lee, S. W. Seo, S. H. Choi and S. H. Im, *Chem. Eng. J.*, 2017, **323**, 153–159.

120 J. Yoon, H. Sung, G. Lee, W. Cho, N. Ahn, H. S. Jung and M. Choi, *Energy Environ. Sci.*, 2017, **10**, 337–345.

121 M. Batmunkh, C. J. Shearer, M. J. Biggs and J. G. Shapter, *J. Mater. Chem. A*, 2016, **4**, 2605–2616.

122 S. Sun, T. Buonassisi and J. Correa-Baena, *Adv. Mater. Interfaces*, 2018, **5**, 1800408.

123 P. Yang, Z. Hu, X. Zhao, D. Chen, H. Lin, X. Lai and L. Yang, *ChemistrySelect*, 2017, **2**, 9433–9437.

124 G. H. Kim, H. Jang, Y. J. Yoon, J. Jeong, S. Y. Park, B. Walker, I. Y. Jeon, Y. Jo, H. Yoon, M. Kim, J. B. Baek, D. S. Kim and J. Y. Kim, *Nano Lett.*, 2017, **17**, 6385–6390.

125 G. Yang, H. Tao, P. Qin, W. Ke and G. Fang, *J. Mater. Chem. A*, 2016, 4, 3970–3990.

126 J. T. W. Wang, J. M. Ball, E. M. Barea, A. Abate, J. A. Alexander-Webber, J. Huang, M. Saliba, I. Mora-Sero, J. Bisquert, H. J. Snaith and R. J. Nicholas, *Nano Lett.*, 2014, **14**, 724–730.

127 G. S. Han, Y. H. Song, Y. U. Jin, J. W. Lee, N. G. Park, B. K. Kang, J. K. Lee, I. S. Cho, D. H. Yoon and H. S. Jung, *ACS Appl. Mater. Interfaces*, 2015, **7**, 23521–23526.

128 X. Zhao, L. Tao, H. Li, W. Huang, P. Sun, J. Liu, S. Liu, Q. Sun, Z. Cui, L. Sun, Y. Shen, Y. Yang and M. Wang, *Nano Lett.*, 2018, **18**, 2442–2449.

129 C. Wang, Y. Tang, Y. Hu, L. Huang, J. Fu, J. Jin, W. Shi, L. Wang and W. Yang, *RSC Adv.*, 2015, **5**, 52041–52047.

130 K. T. Cho, G. Grancini, Y. Lee, D. Konios, S. Paek, E. Kymakis and M. K. Nazeeruddin, *ChemSusChem*, 2016, **9**, 3040–3044.

131 M. M. Tavakoli, R. Tavakoli, P. Yadav and J. Kong, *J. Mater. Chem. A*, 2019, **7**, 679–686.

132 Z. Zhu, J. Ma, Z. Wang, C. Mu, Z. Fan, L. Du, Y. Bai, L. Fan, H. Yan, D. L. Phillips and S. Yang, *J. Am. Chem. Soc.*, 2014, **136**, 3760–3763.

133 A. Agresti, S. Pescetelli, L. Cinà, D. Konios, G. Kakavelakis, E. Kymakis and A. Di Carlo, *Adv. Funct. Mater.*, 2016, **26**, 2686–2694.

134 P. S. Chandrasekhar and V. K. Komarala, *RSC Adv.*, 2017, **7**, 28610–28615.

135 M. M. Tavakoli, R. Tavakoli, S. Hasanzadeh and M. H. Mirfasih, *J. Phys. Chem. C*, 2016, **120**, 19531–19536.

136 M. M. Haley, S. C. Brand and J. J. Pak, *Angew. Chemie Int. Ed. English*, 1997, **36**, 836–838.

137 S. W. Cranford and M. J. Buehler, *Nanoscale*, 2012, **4**, 4587–4593.

138 A. L. Ivanovskii, *Prog. Solid State Chem.*, 2013, **41**, 1–19.

139 H. Du, Z. Deng, Z. Lü, Y. Yin, L. Yu, H. Wu, Z. Chen, Y. Zou, Y. Wang, H. Liu and Y. Li, *Synth. Met.*, 2011, **161**, 2055–2057.

140 C. Kuang, G. Tang, T. Jiu, H. Yang, H. Liu, B. Li, W. Luo, X. Li, W. Zhang, F. Lu, J. Fang and Y. Li, *Nano Lett.*, 2015, **15**, 2756–2762.

141 J. Li, T. Jiu, C. Duan, Y. Wang, H. Zhang, H. Jian, Y. Zhao, N. Wang, C. Huang and Y. Li, *Nano Energy*, 2018, **46**, 331–337.

142 J. Li, N. Wang, F. Bi, S. Chen, C. Zhao, L. Liu, Q. Yao, C. Huang, Y. Xue, H. Liu and T. Jiu, *Sol. RRL*, 2019, **3**, 1900241.

143 L. Yao, M. Zhao, L. Liu, S. Chen, J. Wang, C. Zhao, Z. Jia, S. Pang, X. Guo and T. Jiu, *Mater. Chem. Front.*, , DOI:10.1039/D1QM00592H.

144 J. Xiao, J. Shi, H. Liu, Y. Xu, S. Lv, Y. Luo, D. Li, Q. Meng and Y. Li, *Adv. Energy Mater.*, 2015, **5**, 1401943.

145 J. Li, M. Zhao, C. Zhao, H. Jian, N. Wang, L. Yao, C. Huang, Y. Zhao and T. Jiu, *ACS Appl. Mater. Interfaces*, 2018, **11**, 2626–2631.

146 Y. Guo, Y. Xue, C. Li and X. Li, *Phys. status solidi – Rapid Res. Lett.*, 2020, **14**, 1900544.

147 J. Zhang, J. Tian, J. Fan, J. Yu and W. Ho, *Small*, 2020, **16**, 1907290.

148 H. Li, R. Zhang, Y. Li, Y. Li, H. Liu, J. Shi, H. Zhang, H. Wu, Y. Luo, D. Li, Y. Li and Q. Meng, *Adv. Energy Mater.*, 2018, **8**, 1802012.

149 S. Chen, Q. Pan, J. Li, C. Zhao, X. Guo, Y. Zhao and T. Jiu, *Sci. CHINA Mater.*, 2020, **63**, 2465–2476.

150 F. Bi, C. Yam, C. Zhao, L. Liu, M. Zhao, X. Zheng and T. Jiu, *Phys. Chem. Chem. Phys.*, 2020, **22**, 6239–6246.

151 H. Huang, B. Liu, D. Wang, R. Cui, X. Guo, Y. Li, S. Zuo, Z. Yin, H. Wang, J. Zhang, H. Yuan, L. Zheng and B. Sun, *Nano Res. 2021*, 2021, 1–8.

152 M. A. Khan and M. N. Leuenberger, *Nanophotonics*, 2018, **7**, 1589–1600.

153 T. Akama, W. Okita, R. Nagai, C. Li, T. Kaneko and T. Kato, *Sci. Rep.*, 2017, **7**, 1–10.

154 L. Huang, X. Sun, C. Li, J. Xu, R. Xu, Y. Du, J. Ni, H. Cai, J. Li, Z. Hu and J. Zhang, *ACS Appl. Mater. Interfaces*, 2017, **9**, 21909–21920.

155 V. Gonzalez-Pedro, E. J. Juarez-Perez, W. S. Arsyad, E. M. Barea, F. Fabregat-Santiago, I. Mora-Sero and J. Bisquert, *Nano Lett.*, 2014, **14**, 888–893.

156 J. Burschka, N. Pellet, S. J. Moon, R. Humphry-Baker, P. Gao, M. K. Nazeeruddin and M. Grätzel, *Nature*, 2013, **499**, 316–319.

157 P.-Y. Gu, N. Wang, A. Wu, Z. Wang, M. Tian, Z. Fu, X. W. Sun and Q. Zhang, *Chem. – An Asian J.*, 2016, **11**, 2135–2138.

158 A. A. Said, J. Xie and Q. Zhang, *Small*, 2019, **15**, 1900854.

159 A. A. Said, J. Xie, Y. Wang, Z. Wang, Y. Zhou, K. Zhao, W.-B. Gao, T. Michinobu and Q. Zhang, *Small*, 2019, **15**, 1803339.

160 T. N. Murakami, T. Miyadera, T. Funaki, L. Cojocaru, S. Kazaoui, M. Chikamatsu and H. Segawa, *ACS Appl. Mater. Interfaces*, 2017, **9**, 36708–36714.

161 C. Tao, S. Neutzner, L. Colella, S. Marras, A. R. Srimath Kandada, M. Gandini, M. De Bastiani, G. Pace, L. Manna, M. Caironi, C. Bertarelli and A. Petrozza, *Energy Environ. Sci.*, 2015, **8**, 2365–2370.

162 T. S. Sherkar, C. Momblona, L. Gil-Escrig, J. Ávila, M. Sessolo, H. J. Bolink and L. J. A. Koster, *ACS Energy Lett.*, 2017, **2**, 1214–1222.

163 C. Yang, M. Yu, D. Chen, Y. Zhou, W. Wang, Y. Li, T. C. Lee and D. Yun, *Chem. Commun.*, 2017, **53**, 10882–10885.

164 E. H. Anaraki, A. Kermanpur, L. Steier, K. Domanski, T. Matsui, W. Tress, M. Saliba, A. Abate, M. Grätzel, A. Hagfeldt and J. P. Correa-Baena, *Energy Environ. Sci.*, 2016, **9**, 3128–3134.

165 X. Jia, L. Zhang, Q. Luo, H. Lu, X. Li, Z. Xie, Y. Yang, Y. Q. Li, X. Liu and C. Q. Ma, *ACS Appl. Mater. Interfaces*, 2016, **8**,

18410–18417.

166 Z. L. Tseng, C. H. Chiang and C. G. Wu, *Sci. Rep.*, 2015, **5**, 1–10.

167 J. Song, L. Liu, X. F. Wang, G. Chen, W. Tian and T. Miyasaka, *J. Mater. Chem. A*, 2017, **5**, 13439–13447.

168 J. Song, E. Zheng, J. Bian, X. F. Wang, W. Tian, Y. Sanehira and T. Miyasaka, *J. Mater. Chem. A*, 2015, **3**, 10837–10844.

169 J. Xie, V. Arivazhagan, K. Xiao, K. Yan, Z. Yang, Y. Qiang, P. Hang, G. Li, C. Cui, X. Yu and D. Yang, *J. Mater. Chem. A*, 2018, **6**, 5566–5573.

170 J. Lee, J. Kim, C.-L. Lee, G. Kim, T. K. Kim, H. Back, S. Jung, K. Yu, S. Hong, S. Lee, S. Kim, S. Jeong, H. Kang and K. Lee, *Adv. Energy Mater.*, 2017, **7**, 1700226.

171 A. Giri, G. Park, H. Yang, M. Pal, J. Kwak and U. Jeong, *Adv. Mater.*, 2018, **30**, 1707577.

172 J. M. Yun, Y. J. Noh, J. S. Yeo, Y. J. Go, S. I. Na, H. G. Jeong, J. Kim, S. Lee, S. S. Kim, H. Y. Koo, T. W. Kim and D. Y. Kim, *J. Mater. Chem. C*, 2013, **1**, 3777–3783.

173 M. L. Tsai, S. H. Su, J. K. Chang, D. S. Tsai, C. H. Chen, C. I. Wu, L. J. Li, L. J. Chen and J. H. He, *ACS Nano*, 2014, **8**, 8317–8322.

174 K. Jiao, C. Duan, X. Wu, J. Chen, Y. Wang and Y. Chen, *Phys. Chem. Chem. Phys.*, 2015, **17**, 8182–8186.

175 J. Kang, J. Li, S. S. Li, J. B. Xia and L. W. Wang, *Nano Lett.*, 2013, **13**, 5485–5490.

176 R. Singh, A. Giri, M. Pal, K. Thiyagarajan, J. Kwak, J. J. Lee, U. Jeong and K. Cho, *J. Mater. Chem. A*, 2019, **7**, 7151–7158.

177 H. I. Karunadasa, E. Montalvo, Y. Sun, M. Majda, J. R. Long and C. J. Chang, *Science (80-.).*, 2012, **335**, 698–702.

178 K. Mahmood, A. Khalid, S. W. Ahmad, H. G. Qutab, M. Hameed and R. Sharif, *Sol. Energy*, 2020, **203**, 32–36.

179 Y. J. Huang, H. C. Chen, H. K. Lin and K. H. Wei, *ACS Appl. Mater. Interfaces*, 2018, **10**, 20196–20204.

180 N. A. Abd Malek, N. Alias, S. K. Md Saad, N. A. Abdullah, X. Zhang, X. Li, Z. Shi, M. M. Rosli, T. H. Tengku Abd Aziz, A. A. Umar and Y. Zhan, *Opt. Mater. (Amst).*, 2020, **104**, 109933.

181 M. I. Ahmed, Z. Hussain, A. Khalid, H. M. N. Amin and A. Habib, *Mater. Res. Express*, 2016, **3**, 45022.

182 Y. Wang, S. Wang, X. Chen, Z. Li, J. Wang, T. Li and X. Deng, *J. Mater. Chem. A*, 2018, **6**, 4860–4867.

183 U. Dasgupta, S. Chatterjee and A. J. Pal, *Sol. Energy Mater. Sol. Cells*, 2017, **172**, 353–360.

184 S. Kohnehpoushi, P. Nazari, B. A. Nejand and M. Eskandari, *Nanotechnology*, 2018, **29**, 205201.

185 D. H. Shin, S. H. Shin and S. H. Choi, *Appl. Surf. Sci.*, 2020, **514**, 145880.

186 R. Dai, Y. Wang, J. Wang and X. Deng, *ChemSusChem*, 2017, **10**, 2869–2874.

187 D. Wang, N. K. Elumalai, M. A. Mahmud, H. Yi, M. B. Upama, R. A. Lee Chin, G. Conibeer, C. Xu, F. Haque, L. Duan and A. Uddin, *Synth. Met.*, 2018, **246**, 195–203.

188 A. Agresti, S. Pescetelli, A. L. Palma, A. E. Del Rio Castillo, D. Konios, G. Kakavelakis, S. Razza, L. Cinà, E. Kymakis, F. Bonaccorso and A. Di Carlo, *ACS Energy Lett.*, 2017, **2**, 279–287.

189 Y. Zhou, S. Yang, X. Yin, J. Han, M. Tai, X. Zhao, H. Chen, Y. Gu, N. Wang and H. Lin, *J. Mater. Chem. A*, 2019, **7**, 1878–1888.

190 X. Meng, X. Cui, M. Rager, S. Zhang, Z. Wang, J. Yu, Y. W. Harn, Z. Kang, B. K. Wagner, Y. Liu, C. Yu, J. Qiu and Z. Lin, *Nano Energy*, 2018, **52**, 123–133.

191 N. Arora, M. I. Dar, A. Hinderhofer, N. Pellet, F. Schreiber, S. M. Zakeeruddin and M. Grätzel, *Science (80-.).*, 2017, **358**, 768–771.

192 M. M. Tavakoli, R. Tavakoli, Z. Nourbakhsh, A. Waleed, U. S. Virk and Z. Fan, *Adv. Mater. Interfaces*, 2016, **3**, 1500790.

193 N. Balis, A. A. Zaky, C. Athanasekou, A. M. T. Silva, E. Sakellis, M. Vasilopoulou, T. Stergiopoulos, A. G. Kontos and P. Falaras, *J. Photochem. Photobiol. A Chem.*, 2020, **386**, 112141.

194 T. Umeyama, D. Matano, J. Baek, S. Gupta, S. Ito, V. (Ravi) Subramanian and H. Imahori, *Chem. Lett.*, 2015, **44**, 1410–1412.

195 H. Li, L. Tao, F. Huang, Q. Sun, X. Zhao, J. Han, Y. Shen and M. Wang, *ACS Appl. Mater. Interfaces*, 2017, **9**, 38967–38976.

196 Q. Luo, Y. Zhang, C. Liu, J. Li, N. Wang and H. Lin, *J. Mater. Chem. A*, 2015, **3**, 15996–16004.

197 D. Benetti, E. Jokar, C. H. Yu, A. Fathi, H. Zhao, A. Vomiero, E. Wei-Guang Diau and F. Rosei, *Nano Energy*, 2019, **62**, 781–790.

198 Y. Wang, Y. Hu, D. Han, Q. Yuan, T. Cao, N. Chen, D. Zhou, H. Cong and L. Feng, *Org. Electron.*, 2019, **70**, 63–70.

199 S. Ameen, M. S. Akhtar, M. Nazim, E. B. Kim, M. K. Nazeeruddin and H. S. Shin, *Electrochim. Acta*, 2019, **319**, 885–894.

200 C. C. Chung, S. Narra, E. Jokar, H. P. Wu and E. Wei-Guang Diau, *J. Mater. Chem. A*, 2017, **5**, 13957–13965.

201 S. Feng, Y. Yang, M. Li, J. Wang, Z. Cheng, J. Li, G. Ji, G. Yin, F. Song, Z. Wang, J. Li and X. Gao, *ACS Appl. Mater. Interfaces*, 2016, **8**, 14503–14512.

202 Ç. Şahin, H. Diker, D. Sygkridou, C. Varlikli and E. Stathatos, *Renew. Energy*, 2020, **146**, 1659–1666.

203 A. Capasso, F. Matteocci, L. Najafi, M. Prato, J. Buha, L. Cinà, V. Pellegrini, A. Di Carlo and F. Bonaccorso, *Adv.*

Energy Mater., 2016, **6**, 1600920.

204 Z. Liu, K. Liu, F. Zhang, S. M. Jain, T. He, Y. Jiang, P. Liu, J. Yang, H. Liu and M. Yuan, *Sol. Energy*, 2020, **195**, 436–445.

205 M. Liang, A. Ali, A. Belaidi, M. I. Hossain, O. Ronan, C. Downing, N. Tabet, S. Sanvito, F. EI-Mellouhi and V. Nicolosi, *npj 2D Mater. Appl.*, 2020, **4**, 1–8.

206 G. Kioseoglou, A. T. Hanbicki, M. Currie, A. L. Friedman and B. T. Jonker, *Sci. Rep.*, 2016, **6**, 1–8.

207 L. C. Chen, Z. L. Tseng, C. C. Chen, S. H. Chang and C. H. Ho, *Appl. Phys. Express*, 2016, **9**, 122301.

208 L. B. Chang, C. C. Tseng, J. H. Lee, G. M. Wu, M. J. Jeng, W. S. Feng, D. W. Chen, L. C. Chen, K. L. Lee, E. Popko, L. Jacak and K. Gwozdz, *Vacuum*, 2020, **178**, 109441.

209 L. Huang, N. Huo, Z. Zheng, H. Dong, J. Li, J. Li and J. Li, *J. Semicond.*, 2020, **41**, 52206.

210 Q. Zhou, J. Du, J. Duan, Y. Wang, X. Yang, Y. Duan and Q. Tang, *J. Mater. Chem. A*, 2020, **8**, 7784–7791.

211 S. Li, Z. Chen and W. Zhang, *Mater. Lett.*, 2012, **72**, 22–24.

212 P. Huang, Z. Wang, Y. Liu, K. Zhang, L. Yuan, Y. Zhou, B. Song and Y. Li, *ACS Appl. Mater. Interfaces*, 2017, **9**, 25323–25331.

213 O. J. N. Mesele Hayelom Hailu, Asfafaw Haileslassie Tesfay, Mulu Bayray Kahsay, *An Oil based Indirect Solar Fryer for Injera Baking Application*, 2018.

214 J. Cao, G. Tang, P. You, T. Wang, F. Zheng, J. Zhao and F. Yan, *Adv. Funct. Mater.*, 2020, **30**, 2002358.

215 K. Sobayel, M. Akhtaruzzaman, K. S. Rahman, M. T. Ferdaous, Z. A. Al-Mutairi, H. F. Alharbi, N. H. Alharthi, M. R. Karim, S. Hasmady and N. Amin, *Results Phys.*, 2019, **12**, 1097–1103.

216 A. Kumar and S. Singh, *Mod. Phys. Lett. B*, , DOI:10.1142/S0217984920502589.

217 N. A. A. Malek, N. Alias, A. A. Umar, X. Zhang, X. Li, S. K. M. Saad, N. A. Abdullah, H. Zhang, Z. Weng, Z. Shi, C. Li, M. M. Rosli and Y. Zhan, *Sol. RRL*, 2020, **4**, 2000260.

218 Y. Jeong, D. Shin, J. H. Park, J. Park, Y. Yi and S. Im, *Nano Energy*, 2019, **63**, 103833.

219 Y. Choi, S. Jung, N. K. Oh, J. Lee, J. Seo, U. Kim, D. Koo and H. Park, *ChemNanoMat*, 2019, **5**, 1050–1058.

220 J. Lu, A. Carvalho, H. Liu, S. X. Lim, A. H. Castro Neto and C. H. Sow, *Angew. Chemie*, 2016, **128**, 12124–12128.

221 N. Mahmood, H. Khan, K. Tran, P. Kuppe, A. Zavabeti, P. Atkin, M. B. Ghasemian, J. Yang, C. Xu, S. A. Tawfik, M. J. S. Spencer, J. Z. Ou, K. Khoshmanesh, C. F. McConville, Y. Li and K. Kalantar-Zadeh, *Mater. Today*, 2021, **44**, 69–77.

222 K. A. Messalea, A. Zavabeti, M. Mohiuddin, N. Syed, A. Jannat, P. Atkin, T. Ahmed, S. Walia, C. F. McConville, K. Kalantar-Zadeh, N. Mahmood, K. Khoshmanesh and T. Daeneke, *Adv. Mater. Interfaces*, 2020, **7**, 2001131.

223 V. Krishnamurthi, T. Ahmed, M. Mohiuddin, A. Zavabeti, N. Pillai, C. F. McConville, N. Mahmood and S. Walia, *Adv. Opt. Mater.*, 2021, **9**, 2100449.

224 K. Zhang, L. Zhang, L. Han, L. Wang, Z. Chen, H. Xing and X. Chen, *Nano Express*, 2021, **2**, 12001.

225 F. Li, L. Yang, Z. Cai, K. Wei, F. Lin, J. You, T. Jiang, Y. Wang and X. Chen, *Nanoscale*, 2018, **10**, 20611–20617.

226 K. Meng, S. Gao, L. Wu, G. Wang, X. Liu, G. Chen, Z. Liu and G. Chen, *Nano Lett.*, 2016, **16**, 4166–4173.

227 R. S. Askhadullin, P. N. Martynov, P. A. Yudintsev, A. A. Simakov, A. Y. Chaban, E. A. Matchula and A. A. Osipov, *J. Phys. Conf. Ser.*, 2008, **98**, 72012.

228 P. Tyagi, S. M. Arveson and W. A. Tisdale, *J. Phys. Chem. Lett.*, 2015, **6**, 1911–1916.

229 Y. Wu, L. Wan, S. Fu, W. Zhang, X. Li and J. Fang, *J. Mater. Chem. A*, 2019, **7**, 14136–14144.

230 H. Yu, W. Zhao, L. Ren, H. Wang, P. Guo, X. Yang, Q. Ye, D. Shchukin, Y. Du, S. Dou and H. Wang, *Adv. Mater.*, 2020, **32**, 2001571.

231 Y. Zhang, J. Zhao, J. Zhang, X. Jiang, Z. Zhu and Q. Liu, *ACS Appl. Mater. Interfaces*, 2018, **10**, 15616–15623.

232 K. M. Boopathi, M. Ramesh, P. Perumal, Y.-C. Huang, C.-S. Tsao, Y.-F. Chen, C.-H. Lee and C.-W. Chu, *J. Mater. Chem. A*, 2015, **3**, 9257–9263.

233 O. Yildirim, M. Bonomo, N. Barbero, C. Atzori, B. Civalleri, F. Bonino, G. Viscardi and C. Barolo, *Energies 2020, Vol. 13, Page 5602*, 2020, **13**, 5602.

234 S. Park, M.-S. Kim, W. Jang, J. K. Park and D. H. Wang, *Nanoscale*, 2018, **10**, 4708–4717.

235 M. G. Mohamed, C.-C. Lee, A. F. M. EL-Mahdy, J. Lüder, M.-H. Yu, Z. Li, Z. Zhu, C.-C. Chueh and S.-W. Kuo, *J. Mater. Chem. A*, 2020, **8**, 11448–11459.

236 T.-H. Chang, C.-W. Kung, H.-W. Chen, T.-Y. Huang, S.-Y. Kao, H.-C. Lu, M.-H. Lee, K. M. Boopathi, C.-W. Chu and K.-C. Ho, *Adv. Mater.*, 2015, **27**, 7229–7235.

237 H.-Y. Chung, C.-H. Lin, S. Prabu and H.-W. Wang, *J. Chinese Chem. Soc.*, 2018, **65**, 1476–1481.

238 U. Ryu, S. Jee, J.-S. Park, I. K. Han, J. H. Lee, M. Park and K. M. Choi, *ACS Nano*, 2018, **12**, 4968–4975.

239 Y. N. Zhang, B. Li, L. Fu, Q. Li and L. W. Yin, *Electrochim. Acta*, 2020, **330**, 135280.

240 X. Zhao, J. Zhao, J. He, B. Li, Y. Zhang, J. Hu, H. Wang, D. Zhang and Q. Liu, *ACS Appl. Energy Mater.*, 2020, **3**, 6180–6187.

241 J. Ji, B. Liu, H. Huang, X. Wang, L. Yan, S. Qu, X. Liu, H. Jiang, M. Duan, Y. Li and M. Li, *J. Mater. Chem. C*, 2021, **9**, 7057–7064.

242 M. Li, J. Wang, A. Jiang, D. Xia, X. Du, Y. Dong, P. Wang, R. Fan and Y. Yang, *Sol. Energy*, 2019, **188**, 380–385.

243 L. Huang, X. Zhou, R. Wu, C. Shi, R. Xue, J. Zou, C. Xu, J. Zhao and W. Zeng, *J. Power Sources*, 2019, **433**, 226699.

244 J. Zhang, S. Guo, M. Zhu, C. Li, J. Chen, L. Liu, S. Xiang and Z. Zhang, *Chem. Eng. J.*, 2021, **408**, 127328.

245 X. Zhou, L. Qiu, R. Fan, J. Zhang, S. Hao and Y. Yang, *Nano-Micro Lett. 2020 121*, 2020, **12**, 1–11.

246 M. Seifpanah Sowmehesaraee, M. Ranjbar, M. Abedi and S. A. Mozaffari, *Sol. Energy*, 2021, **214**, 138–148.

247 S. Gbadamasi, M. Mohiuddin, V. Krishnamurthi, R. Verma, M. W. Khan, S. Pathak, K. Kalantar-Zadeh and N. Mahmood, *Chem. Soc. Rev.*, 2021, **50**, 4684–4729.

248 N. Mahmood, I. A. De Castro, K. Pramoda, K. Khoshmanesh, S. K. Bhargava and K. Kalantar-Zadeh, *Energy Storage Mater.*, 2019, **16**, 455–480.

249 Y. Zhu, W. Peng, Y. Li, G. Zhang, F. Zhang and X. Fan, *J. Mater. Chem. A*, 2019, **7**, 23577–23603.

250 Y. Liu, Y. Huang and X. Duan, *Nat. 2019 5677748*, 2019, **567**, 323–333.

251 A. Koma, K. Sunouchi and T. Miyajima, *Microelectron. Eng.*, 1984, **2**, 129–136.

252 A. Koma, *J. Cryst. Growth*, 1999, **201**–**202**, 236–241.

253 M. Yankowitz, Q. Ma, P. Jarillo-Herrero and B. J. LeRoy, *Nat. Rev. Phys. 2018 12*, 2019, **1**, 112–125.

254 C. Zhang, C.-P. Chuu, X. Ren, M.-Y. Li, L.-J. Li, C. Jin, M.-Y. Chou and C.-K. Shih, *Sci. Adv.*, 2017, **3**, e1601459.

255 J. Kang, J. Li, S.-S. Li, J.-B. Xia and L.-W. Wang, *Nano Lett.*, 2013, **13**, 5485–5490.

256 S.-Y. Xie, X.-B. Li, W. Q. Tian, N.-K. Chen, Y. Wang, S. Zhang and H.-B. Sun, *Phys. Chem. Chem. Phys.*, 2014, **17**, 1093–1098.

257 X. Ma, D. Jiang, P. Xiao, Y. Jin, S. Meng and M. Chen, *Catal. Sci. Technol.*, 2017, **7**, 3481–3491.

258 H. Wang, L. Zhang, Z. Chen, J. Hu, S. Li, Z. Wang, J. Liu and X. Wang, *Chem. Soc. Rev.*, 2014, **43**, 5234–5244.

259 K. Xu, Y. Xu, H. Zhang, B. Peng, H. Shao, G. Ni, J. Li, M. Yao, H. Lu, H. Zhu and C. M. Soukoulis, *Phys. Chem. Chem. Phys.*, 2018, **20**, 30351–30364.

260 J. Su, G.-D. Li, X.-H. Li and J.-S. Chen, *Adv. Sci.*, 2019, **6**, 1801702.

261 J. Low, J. Yu, M. Jaroniec, S. Wageh and A. A. Al-Ghamdi, *Adv. Mater.*, 2017, **29**, 1601694.

262 F. Withers, O. Del Pozo-Zamudio, A. Mishchenko, A. P. Rooney, A. Gholinia, K. Watanabe, T. Taniguchi, S. J. Haigh, A. K. Geim, A. I. Tartakovskii and K. S. Novoselov, *Nat. Mater. 2014 143*, 2015, **14**, 301–306.

263 S. J. A. Moniz, S. A. Shevlin, D. J. Martin, Z.-X. Guo and J. Tang, *Energy Environ. Sci.*, 2015, **8**, 731–759.

264 K. Zhang, T. Zhang, G. Cheng, T. Li, S. Wang, W. Wei, X. Zhou, W. Yu, Y. Sun, P. Wang, D. Zhang, C. Zeng, X. Wang, W. Hu, H. J. Fan, G. Shen, X. Chen, X. Duan, K. Chang and N. Dai, *ACS Nano*, 2016, **10**, 3852–3858.

265 A. T. Hanbicki, H.-J. Chuang, M. R. Rosenberger, C. S. Hellberg, S. V Sivaram, K. M. McCreary, I. I. Mazin and B. T. Jonker, *ACS Nano*, 2018, **12**, 4719–4726.

266 Y. Liu, S. Zhang, J. He, Z. M. Wang and Z. Liu, *Nano-Micro Lett. 2019 111*, 2019, **11**, 1–24.

267 Y. Liu, N. O. Weiss, X. Duan, H.-C. Cheng, Y. Huang and X. Duan, *Nat. Rev. Mater. 2016 19*, 2016, **1**, 1–17.

268 X.-H. Li and M. Antonietti, *Chem. Soc. Rev.*, 2013, **42**, 6593–6604.

269 T. Kwon, M. Jun, J. Joo and K. Lee, *J. Mater. Chem. A*, 2019, **7**, 5090–5110.

270 Z. Hu, Z. Wu, C. Han, J. He, Z. Ni and W. Chen, *Chem. Soc. Rev.*, 2018, **47**, 3100–3128.

271 K. Chu, Y. Liu, Y. Li, Y. Guo and Y. Tian, *ACS Appl. Mater. Interfaces*, 2020, **12**, 7081–7090.

272 Y. Yu, J. Zhou and Z. Sun, *Nanoscale*, 2019, **11**, 23092–23104.

273 R. Li, W. Sun, C. Zhan, P. R. C. Kent and D. Jiang, *Phys. Rev. B*, 2019, **99**, 85429.

274 X. Fang, X. Yu, S. Liao, Y. Shi, Y. S. Hu, Z. Wang, G. D. Stucky and L. Chen, *Microporous Mesoporous Mater.*, 2012, **151**, 418–423.

275 E. Pomerantseva and Y. Gogotsi, *Nat. Energy 2017 27*, 2017, **2**, 1–6.

276 C. N. R. Rao, K. Pramoda, A. Saraswat, R. Singh, P. Vishnoi, N. Sagar and A. Hezam, *APL Mater.*, 2020, **8**, 20902.

277 K. Pramoda, U. Gupta, M. Chhetri, A. Bandyopadhyay, S. K. Pati and C. N. R. Rao, *ACS Appl. Mater. Interfaces*, 2017, **9**, 10664–10672.

278 K. Pramoda, S. Servottam, M. Kaur and C. N. R. Rao, *ACS Appl. Nano Mater.*, 2020, **3**, 1792–1799.